Beachrocks and lithified barriers in the Gulf of Lions (western Mediterranean Sea) as new markers of the last sea-level rise

Pierre Giresse, Serge Berné, Raphaël Certain, Thierry Courp, Bertil Hebert, Olivier Raynal

Sedimentology
February 2023, Volume 70, Issue 2, Pages 569-591
https://doi.org/10.1111/sed.13061
https://archimer.ifremer.fr/doc/00804/91612/

Beachrocks and lithified barriers in the Gulf of Lions (western Mediterranean Sea) as new markers of the last sea-level rise

Giresse Pierre [1, *], Berné Serge [1], Certain Raphael [1], Courp Thierry [1], Hebert Bertil [1], Reynal Olivier [1]

[1] Centre de Formation et de Recherche sur les Environnements Méditerranéens (CEFREM), UMR CNRS 5110, Université de Perpignan Via Domitia, Avenue Paul Alduy, Perpignan 66000, France

* Corresponding author : Pierre Giresse, email address : giresse@univ-perp.fr

Abstract :

The Gulf of Lions shelf (southern part of the French Mediterranean coast) displays several occurrences of beachrocks, thus offering an exceptional opportunity to determine the stages of the last marine transgression. These beachrocks crop out especially on the outer shelf and near the modern shoreline. In addition, several other exposures are located on the inner shelf between 10 m and 25 m). The absence of exposure on the middle shelf (water depths of 25 to 90 m) is probably related to a higher rate of sea-level rise. Most of the beachrocks occur at the top of two or three parallel and contiguous barriers. The seaward barriers are generally less lithified than the inner barriers. Each barrier displays an asymmetric profile, the seaward slope being more accentuated. This gently-dipping landward slope forms part of the outer trough resulting from resuspension due to enhanced turbulence at the barrier toe. Almost all of these beachrocks are coarse quartz-rich sandstones and conglomerates, whose large pore space has been first filled by magnesian calcite (ca 11 mol.% MgCO3), which predominantly fills the voids. Secondary sparites or microsparites, also composed of high-magnesian calcite, may develop locally in the last remaining voids. Finally, more rarely and very locally (for example, Pierres de Sète), a late-stage cementation of low-magnesian calcite is observed which expresses a brief episode of influence from a nearby freshwater groundwater table. δ18O and δ13C values reflect the relative geochemical homogeneity of these Gulf of Lions beachrocks. However, they are quite distinct from other marine cements, and in particular, those of the eastern Mediterranean, expressing lower temperatures and a lack of influence of dissolved carbon linked to terrigenous fluxes. Based on the radiocarbon ages of these calcitic cements, this study proposes new index points on sea-level positions in the Gulf of Lions from -95 to 108 m to -0.3 m water depths, between ca 18,583 a cal BP and 633 a cal BP.

Keywords : Beachrock, cementation, Gulf of Lions shelf, lithified barrier, magnesian calcite, sea-level rise

INTRODUCTION

Sea-level changes during the late Quaternary glacial periods are generally inferred from the isotopic composition of marine foraminifera (Shackleton, 1987; Waelbroeck *et al.,* 2002; Siddall *et al.*, 2003), the U/Th dating of coral reefs (Bard, 1996) or the position of palaeo-shorelines (Rabineau *et al.*, 2006). There is a general agreement that beachrocks are valuable tools for reconstructing sea-level changes (i.e. Mauz *et al.,* 2015; Rovere *et al.*, 2016; Falkenroth *et al.*, 2019). they provide compaction-free index points, rare among reworked material (Vacchi *et al.*, 2016). Beachrocks are intertidal deposits forming in the zone where carbonate-saturated meteoric and marine water mix and pCO_2 decreases. Vousdouskas *et al.* (2007) have provided a synthesis of the mechanisms of beachrock formation.

On the continental shelf of the Gulf of Lions (GoL), a succession of submerged beachrocks provides a rare opportunity to reconstruct sea-level changes at the scale of the last glacio-eustatic cycle. Pleistocene lithified sandstones were identified at the outer edge of the shelf by Rabineau (2001) and named 'Pierres de Sète' following the name employed by local

fishermen. These barrier deposits form a crescentic 'ridge' between 108 m and 90 m water depth and are interpreted by the same authors as regressive littoral units deposited during the sea-level fall induced by the last glaciation.

More recently, divers have sampled Holocene lithified sediments from the inner shelf and nearshore areas of the southern GoL. These samples were collected from ridges culminating at water depths of 25 m (Fayté), 23 m (Saint-André), 20 m (Tavac), 10 m (Racou) and 0.3 to 0.4 m (Leucate) (Fig. 1).

This study describes new samples from 0.35 to 25 m water depth, as well as two samples situated at 95 m ± 5 m (Pierres de Sète) already dated by Mauffrey *et al.* (2015). The lithological facies and microfacies, as well as the mineralogy and the geochemistry of the cements are described. Crystals from the new samples were sub-sampled for ^{14}C dating of sandstone cementation in the same way as for the Pierres de Sète samples. This allows for more precise measurements to be obtained and compared with previous studies only based on mollusc shells (Aloïsi *et al*., 1978).

REGIONAL SETTING AND LOCAL STUDIES ON PAST SEA-LEVEL CHANGES

At present, the GoL, situated in the Western Mediterranean basin, is a relatively low-energy shelf. The tidal range is less than 30 cm (Pirazzoli *et al*., 2007), while the most energetic waves are generated during less than 0.1% of the time by winds from the east or south-east (north-westward swells up to 10 m high associated with periods of *ca* 12 s; Dufois *et al.,* 2014).

General circulation in the GoL is related to the Liguro–Provençal current, flowing south-westward along the continental slope (Millot, 1990). This general circulation and the longshore drift are responsible for the development of the continental shelf to the west of the Rhône River, which represents the major source of sediment for this shelf (mainly coming from the Alps) (Guieu *et al*., 1991).

Large sand bodies, formerly called *'sables du large'* ('offshore sands') by Bourcart (1945), occur at depths ranging from 80 to 100 m and cover a large part of the outer shelf. Seismic investigations show that these offshore sands are prograding units, up to 35 m thick, with seaward dipping clinoforms. Based on these observations and the ^{14}C dating of shallow cores, various authors have interpreted these sands as regressive littoral units deposited during sea-level fall induced by the last glaciation (Berné *et al.*, 1998; Rabineau, 2001; Rabineau *et al.*, 2005).

Deglacial and Holocene sediments are irregularly distributed over the shelf, forming a thick wedge (up to 40 m) on the inner shelf in the vicinity of the Rhône delta (Aloïsi *et al.*, 1975), which pinches out seaward at depths of 60 to 90 m (Got & Aloïsi, 1990; Gensous & Tesson, 1997; Labaune *et al.*, 2005). A series of transgressive parasequences was also identified on the mid-shelf (50 to 70 m), the best-preserved being linked to a slowdown of sea-level rise during the Younger Dryas (Berné *et al.*, 2007). Landward, a more recent parasequence assigned to the 8.2 kyr cooling event was observed in boreholes on the Rhône delta plain (Amorosi *et al.*, 2013). This parasequence was also identified in the offshore domain on long piston cores of the modern prodelta (Fanget *et al.*, 2014).

Previous studies on palaeo-sea-levels in the Gulf of Lions

Along the coastline, GPS-derived vertical velocities indicate zero vertical movements over most of the GoL and the elevation of the MIS5e shoreline corroborates long-term stability of the area (Vacchi *et al.*, 2016), at least for the period considered in this study. An averaged long-term (Plio-Pleistocene) subsidence of 240 ± 15 m/Myr is estimated at the shelf edge (Rabineau *et al.*, 2014). In detail, Jouet *et al.* (2008) used forward stratigraphic modelling to evaluate the different components of subsidence during the last climatic cycle (125 kyr). Jouet *et al.* (2008) found that, at the shelf edge (about 100 km of the modern shoreline), the major driver of subsidence is water loading. Since the Last Glacial Maximum, it caused subsidence on the order of 20 m (Jouet *et al.*, 2008).

The first attempt to determine the sea-level evolution in the western Gulf of Lions was done by

Labeyrie *et al.* (1976).

These authors used a set of cores to determine the transition between continental and marine deposits, in order to track the flooding of the emerged shelf during the Deglacial – Holocene. They dated the marine shells that post-dated the period of inundation. The same method was employed by Aloïsi (1986) for the entire Gulf of Lions. Using the well-preserved topsets of an early Rhône deltaic complex (Younger Dryas to Preboreal in age), Berné *et al*. (2007) determined two sea-level index points at depths between 50 m and 55 m.

More recently, Vacchi *et al.* (2016) re-interpreted already published samples from the western Mediterranean Sea from various deposits (marsh and lagoonal deposits, fixed organisms, beachrocks, archaeological remains) in order to produce a multi-proxy data base. For the French Mediterranean area, most of their index points are from the Rhône deltaic plain.

Recently, boreholes were drilled onshore in the Narbonne area, north of the study area. Salel *et al.* (2020) used marine shells and organic material to post-date the flooding of a palaeo-estuary and palaeo-lagoon systems, as well as continental peat as pre-flooding marker. They obtained a relative sea-level curve for the 9.5 to 6 ka cal BP interval.

The first attempt to use beachrocks as sea-level markers was used by Jouet *et al*. (2006) and Maufrey *et al.,* (2015). As the same samples are re-analyzed here, the results of these authors will be discussed in the following sections.

A compilation of these results and a comparison with this study's data will be presented in the *Discussion*.

SAMPLING AND METHODS

Operations at sea

On the inner shelf (-10 to -25 m water depth), lithified sediments were sampled by divers at the top of some of the previously known hard-rock by fishermen ('2' to '5' in Fig. 1; Table 1). The water depth of sampling was measured by divers with a calibrated depth gauge. Additional samples from deep (about -95 m) samples of Mauffrey *et al*. (2015) are included in this study ('1' in Fig. 1), as well as two samples ('6' and '7' in Fig. 1) from a very shallow (-0.35 m) lithified barrier off Leucate Beach.

During the 2010 CAP 66 campaign, swath bathymetric surveys, together with acoustic imaging, were carried out on the inner shelf using the IFREMER coastal vessel 'Haliotis'. This small vessel is equipped with a Geoswath Plus™ interferometric sonar (Kongsberg Maritime, Kongsberg, Norway). The device functions at a frequency of 250 kHz and provides bathymetry and imaging measurements (amplitude of backscatter signal). The vessel is also equipped with a hull-mounted IFREMER Subop sub-bottom profiler. The receiver array is separate from the transmitter array to ensure operation in very shallow waters, while using frequency-modulated signals of suitable duration (1700 to 5500 Hz from 10 to 50 ms). It uses a low-frequency sonar system that provides excellent vertical resolution and can acquire data at vessel speeds of up to 7 knots.

Side-scan sonar data were collected by means of a dual-frequency (325/780 kHz) C-Max CM2™ towfish (C-Max Limited, Dorchester, UK). The side-scan sonar data were recorded and processed using HYPACK™ software.

On the outer shelf, an SIG France™ sparker (SIG France, Bouvron, France) was utilized with a power ranging from 100 to 700 Joules and shooting rates between 1.0 s and 0.5 s. Data were acquired with a Delph™ system and incorporated into a large database under IHS-Kingdom Suite™.

Mineralogical and geochemical analysis

Some calcitic cement was separated from the bulk sediment of each site, with specimens being mounted, polished, thinly coated with gold and then morphologically examined using a HITACHI S 4500 scanning electron microscope (SEM) fitted with an energy dispersive X-ray (EDX) microprobe (Tracor system) (Hitachi High-Tech Corporation, Tokyo, Japan). Bulk chemical data were obtained by spot analysis of selected crystals over an area of 50 µm x 50 µm. A beam-diameter of *ca* 1 µm gives an interaction volume of *ca* 8 µm, so the spot analysis can therefore be regarded as the average composition of the volume. EDX analyses of the Mg-content of diagenetic crystals were obtained from an EDX-PGT instrument (Princeton Gamma-Tech, Princeton, NJ, USA) using an energy of 5 Kev (kiloelectronvolt) for a density of 2.75, providing a resolution of 0.4 µm (pear-shaped interaction volume).

The mineral composition of the calcitic cement was studied by X-ray diffraction (XRD; Philips 1729/1759, Malvern Panalytical, Malvern™, UK). Samples of about 100 mg of handpicked cement fragments were analysed using Cu Kα radiation. The mole percentage (mol. %) $MgCO_3$ in the calcite cement samples was estimated by measuring the position of the d(211) peak according to the Goldsmith *et al.* (1961) curve used by Mackenzie *et al.* (1983) and Fahad & Saeed (2018).

The $\delta^{18}O$ and $\delta^{13}C$ measurements were performed using a Finnigan MAT 253 mass spectrometer connected to a Kiel IV carbonate device (Thermo Fisher Scientific, Waltham, MA, USA) at the Institut Universitaire d'Etudes Marines (IUEM) Stable Isotope Laboratory (Brest). Data are reported in standard δ-notation *versus* VPDB. Analytical precision on stable isotopes is $<\pm 0.05‰$ for $\delta^{18}O$ and $<\pm 0.02‰$ for $\delta^{13}C$.

Preparation of cements for radiocarbon dating

Various dates have been obtained from calcareous cements in marine sediments, especially Holocene beachrocks, and used to reconstitute sea-level changes (Ramsay & Cooper, 2002; Desruelles *et al.,* 2009). Although cements can be contaminated by carbonate particles other

than the calcite cement, radiocarbon ^{14}C is still the most appropriate method for dating beachrocks.

After grinding the sample, siliciclastic and quartz grains were separated from calcareous grains using bromoform (density = 2.85 g/cm^3). By adjusting the density with acetone, this heavy liquid was used to separate floating quartz grains from sinking calcitic grains (cement fragments, lithoclasts and bioclasts). In a subsequent step, the remaining aggregates were picked and then slowly and gently ground in order to separate the micritic cement from the quartz crystals (Fig. 2). Some cements are partially composed of low-magnesian calcite (Pierres de Sète, Leucate). It represents the last episode of cementation, which occurs in small quantities and in the outer (or border) areas of the beachrock. These cements were removed from the sample and were not dated.

The ^{14}C ages reported here are based on this extracted material and were determined at the Laboratoire de Mesure du Carbone 14 (LMC14) using the ARTEMIS ^{14}C Acceleration Mass Spectrometer (AMS) National Facility based at the CEA site in Saclay (France) (Moreau *et al.*, 2020). Samples were washed in an acid solution (HNO_3 10^{-2} M) for 15 mn. The pre-treatment and graphitization steps were carried out following the procedure described in detail by Dumoulin *et al.* (2017). This study uses the Marine20 curve of the CALIB 8.2 calibration programme (Stuiver *et al.*, 2020), where the modern global ocean age is modelled at 550 years instead of 400 years, along with a local correction. An averaged regional marine radiocarbon reservoir age correction ΔR of -43 was applied, as well as an averaged uncertainty of 45 for the Marine 20 calibration, based on Siani *et al.* (2000). The same corrections are applied to the ^{14}C ages of samples already studied/published. All ages mentioned below are in calibrated years before present (a or ka cal BP), except when specifically mentioned.

In addition to the new data set, included here are previously published results for the Pierres de Sète samples (Mauffrey *et al.*, 2015), since the same technique was used to extract the cement. On the other hand, all other previous ^{14}C ages based on bulk sediment samples or mollusc shells were excluded (see *Discussion*).

Determination of Sea-Level Index Points (SLIP)

As summarized by Mauz *et al.* (2015), a SLIP is defined by: (i) the location of the sample; (ii) its age; (iii) the sampling elevation; and (iv) the known relationship between the indicator and the corresponding shoreline. In the current case, the location error is less than 1 m for coastal samples ('6' and '7' in Fig. 1), in the order of 10 m for samples 2 to 5. In any event, what matters is the accuracy of the sampling elevation (see below). The age error corresponds to the 2 s error on the age of the sample determined by AMS radiocarbon dating. Regarding the elevation, this study follows the conservative approach of Vacchi *et al.* (2016) was followed, where the indicative range of beachrocks is +1 m and -2 m with respect to mean sea-level (MSL). According to Shennan & Horton (2002), the total vertical error includes the sum of quantified or estimated errors (including the indicative range) as:

$$e = (e_1^2 + e_2^2 + \ldots + e_n^2)^{1/2} \qquad \text{Eq.1}$$

For samples obtained directly on the beach, the total error is mainly related to the indicative range. For samples obtained by divers, the total error mainly depends on the accuracy of the diving gauge (in the order of ±1 m) and on the indicative range.

In the case of the Pierres de Sète, the dredging technique did not allow determination of the precise position of the samples. The depth of the samples was evaluated from the track of the dredge on the bathymetric map (Fig. 3). Therefore, the study considered the intercept of the track of the dredge with the entire ridge (between -90 m that marks the top of the ridge, and the deepest contour line crossed by the dredge at about -100 m). This yields a very conservative total vertical error of approximatively ±5 m for the Pierres de Sète.

The results are plotted as rectangles on the Age/Relative sea-level curve, where the horizontal corresponds to the 2σ error on the calibrated age and the vertical is the sum of errors as defined above.

MORPHOLOGICAL CHARACTERISTICS OF THE SAMPLED AREAS

Outer shelf: Pierres de Sète

The Pierres de Sète barrier (1 in Fig. 1; Table 1) runs parallel to the 100 m isobath and rises from the surrounding seafloor by up to 20 m. The swath bathymetric map (Fig. 3) shows that, on average, the barrier has a lateral extent of more than 7 km and a width of about 300 m. As such, it is the largest morphological feature of the entire GoL continental shelf. To the north-east, the ridge divides into two parallel units separated by about 250 m, each of them having approximately the same height and width. In addition to the main unit, a set of isolated highs extends to the south of the Pierres de Sète. Taken together, the relief has a lateral extent of more than 10 km and is parallel to the wave-cut notch forming the seaward limit of the offshore sands left by the last sea-level fall. It might correspond to a palaeo-sand spit. The bathymetric map also reveals circular or elliptic depressions contiguous to the landward (north-west) flank of the relief, with a negative topography of up to 6 m.

Seismic data show that the Pierres de Sète lies on top of the prograding sands, near their seaward limit (Fig. 4). The seismic data also clearly shows that the present-day topography of the Pierres de Sète (up to 20 m above the present-day sea floor) is due to differential erosion, as demonstrated by the angular termination of underlying clinoforms and the erosional depressions along the north-west flank of the relief (that are also at the origin of circular depressions situated to the north of the barrier). It is likely that the beachrocks acted as a shield against erosion, being at the origin of the elongated relief.

Inner shelf

The lithified sands lie on top of narrow and few metre high barriers

Fayté ('2' in Figs 1 and 5A; Table 1)

This feature forms a narrow and discontinuous 2 m high barrier, parallel to the isobaths, 750 m long and 20 to 40 m wide, culminating at a water depth of 25 m. It reaches about 2 m above the

surrounding sea floor. The vertical profile is generally asymmetrical, with a steeper slope on the landward compared to the seaward flank.

Saint-André ('3' in Figs 1 and 5B; Table 1)

There are three main small outcrops, about 1 m high, 100 m long and 30 m wide. They are aligned along the 23 m isobath, suggesting that they correspond the remains of a previous, more developed, barrier that was buried beneath the prograding late Holocene sediments.

Tavac ('4' in Figs 1 and 5C; Table 1)

The outcrops form an 880 m long and 30 to 50 m wide barrier, lying at about 20 m depth. They form rather discontinuous reliefs, about 3 m high above the surrounding sea floor. The slope is steeper on the seaward than on the landward side.

Racou ('5' in Figs 1 and 6; Table 1)

These cemented sands are rooted on Precambrian siliceous shales, clearly visible on the bathymetric map which form the bedrock for sandstone cementation. Two bathymetric profiles (1 and 2) perpendicular to the alignment of beachrock outcrops reveal the presence of two barriers, 1.5 to 2.0 m high with respect to the surrounding sea floor. They are 375 m and 200 m long, respectively, and 40 to 30 m wide, with a more accentuated slope on the landward flank. Only the deepest outcrop was sampled, at a water depth of 10 m.

Beachrocks on the recent coastline (Leucate)

Leucate ('6' – '7' in Figs 1 and 7; Table 1)

The white-yellowish sandstone of Leucate forms a shore parallel barrier, about 1.5 m thick and with a lateral extent in the order of 10 km. In detail, there are two or three lithified strata with a *seaward dipping* reaching about 6°, separated by unconsolidated sands. Only the shallowest

strata was sampled (at 0.35 m water depth) in a place where it is well consolidated (sample L1), and another where the cementation was too weak to allow consolidation of the rock (sample L2).

MACROSCOPIC CHARACTERISTICS OF THE GULF OF LIONS BEACHROCKS

Outer shelf: Pierres de Sète

Sampling was carried out at depths between 100 m and 90 m below present-day sea-level (see *Sampling and methods*). The samples consist of cemented coarse siliceous sand with grains arranged obliquely to the presumed erosion surface, which is recognized as a dark and undulating surface. The smallest quartz grains are beige-yellowish, and their oblique arrangement is picked out by black to brownish coarser heavy minerals (>2 mm). The deposits are medium-bedded (10 cm thick parallel beds or laminae), suggesting a relatively high-energy environment (large-scale cross beds or upper planar beds) (Fig. 8A) as observed in some other beachrocks (Mauz *et al.,* 2015, fig. 1). They display a distinct fining-upward sequence toward the rock surface that is often corroded and colonized by recent encrusting organisms.

Inner shelf

Fayté

The sample is generally a conglomerate characterized by moderately rounded and poorly sorted clasts; 5 to 50 mm quartz gravels are associated with 0.3 to 0.5 mm sand grains. Other clasts are several millimetres in size and formed of mica schists or sometimes micro-sandstones (Fig. 8B). In some places, quartz clasts are nearly contiguous, and the cementation is almost complete.

Saint-André

The sample is a quartz-rich sandstone including several 0.5 to 1.0 cm dark grey clasts often elongated (schistous structure, sometimes mica schistous or gneissic) and some carbonate

bioclasts. Rounded quartz grains (about 1 mm in diameter) are well-sorted. The rock surface is partly covered with serpulid and bryozoan encrustations.

Tavac

The sample is a micro-conglomerate with rare sandy and gravelly layers showing very poor sorting (Fig. 8C). Extremely well-rounded pebbles, 0.5 to 2 or 3 cm in size, are of heterogeneous composition: white or bluish siliceous sandstone, gneisses (including a 4 cm pebble), shales and mica schists. The pebbles were in close contact and form a rigid framework.

Racou

The sawn surface of the sample reveals a sandy conglomerate, poorly sorted with some 1 cm gravel layers associated with coarse sand; this lithology bears some resemblance to the gravel-stones of Tavac (Fig. 8D). The well-rounded pebbles are composed of quartz (up to 1 cm), gneisses, schists and mica schists. The cement is slightly porous with several narrow openings, sometimes highly oxidized.

Coastal beachrocks (Leucate)

The sampled deposits correspond to multi-layered beds, about 10 cm thick, dipping gently seaward and including marked discontinuity surfaces. Several beds display fining-upward sequences, passing from gravelly-sandy to coarse to fine sandy units, the coarsest laminae being picked out by heavy mineral concentrations. The coarse sand fraction is composed of rounded quartz grains 1 to 2 mm in size that are almost contiguous. Dark rounded grains of Albian siltstones or mica schist debris are sometimes associated with various shell remains. At the shallowest outcrop, these sandstones show various degrees of cementation at the scale of 100 m. Some sandstones occur as strongly cemented slabs without residual porosity (sample L1), while others are poorly cemented with weakly bound friable micrites (sample L2) (Fig. 8E and F).

MICROSCOPIC OBSERVATIONS

Pierres de Sète

The sandstone consists mainly of siliciclastic grains (65 to 85%) (Fig. 9A). Dominant quartz is associated with heavy minerals, feldspars, siliceous rocks (quartzite, radiolarite, shale, gneiss). Minor carbonate grains (10 to 15%) include bioclasts (urchin spines, bivalves, bryozoans) and micritic grains (intraclasts formed *in situ* and lithoclasts). The cement consists of isopachous rims of microsparite around all the grains, with rim thickness varying from 6 to 15 µm. The resulting network defines a fairly high porosity.

Scanning electron microscope analysis shows that the grains are completely surrounded by radiaxial prismatic $CaCO_3$ crystals, 5 to 10 µm long, arranged in a regular palisade texture. These crystals are small and elongate but relatively stocky (scalenohedrons). The prismatic rhomb shape of the euhedral to anhedral crystals corresponds to c-axis growth (Fig. 10A), generally oriented perpendicular to the substrate. Locally, these prismatic crystals are preceded by a discrete micritic coating 1 to 2 µm thick (first layer) that does not cover the grains regularly (Fig. 10B).

Fayté

The cement is commonly micritic, dark and homogeneous, probably expressing a single phase of almost complete filling. Similarly to the Pierres de Sète beachrock, dark micritic coatings are observed around schistous sandstone clasts (Fig. 9B). Patches of transparent acicular crystals occur within the micrite and form a major part of the late-stage generation of needle-shaped crystals that splay into the pore space. As a result of the high concentration of siliceous debris, the bulk carbonate content reaches only 10.8%.

Saint-André

The cement texture is essentially microcrystalline. However, some microsparitic patches may have developed in the final stages of cavity filling, i.e. the chambers of benthic foraminifera are also seen in small depressions on the quartz surface (Fig. 9C). The significant development of cement accounts for a carbonate content reaching 37%.

Tavac

Examination at high magnification indicates, as at Fayté, the practically ubiquitous character of microcrystalline cementation, which sometimes incrusts the surficial fissures of quartz grains. Note the presence of brown coatings and denser, darker binding phases with some microsparitic patches. Successive micritic and microsparitic accumulations are observed on a quartz grain (Fig. 10C). The bulk carbonate content reaches 22.1%.

Racou

Homogeneous microcrystalline cement is common over the entire surface (Fig. 9D). It continuously borders the clasts; progressively decreasing toward the rim, becoming lighter or almost transparent in polarized light. It is noteworthy that the cementation is not developed in some parts of the section. The fairly abundant cement accounts for a carbonate content of the bulk rock reaching 19%.

Leucate

In the well-cemented sample (L1), the texture of the microcrystalline cement is largely homogeneous, and the resulting pore space is very restricted. The most common arrangement is an initial uneven dark micritic film followed by a dominant microsparitic accumulation; the particular character of this cementation is that it is not observed in other samples, except in the

Pierres de Sète. The second sample (L2) is poorly cemented with friable micrite occurring as weakly bound aggregates of very small crystals (<2 µm). Locally, the binding is ensured by uneven coatings at the level of the contact points of the grains. These Leucate beachrocks are almost devoid of shell clasts. This uneven cementation accounts for a fairly low overall carbonate content (about 9.3%).

In summary, three stages of cementation are suggested.

1 Dark micrites formed fairly rapidly at first, but with more or less incomplete cementation, resulting in a friable to very friable sandstone (L2).

2 Microcrystalline crystals formed an initial rim followed by some microsparites (L1).

3 In addition to the two previous stages, patches of transparent acicular crystals occur within the micrite and form a major part of the latest generation of needle-shaped crystals as seen in the Fayté beachrock. This results in a very hard sandstone.

MINERALOGICAL AND GEOCHEMICAL CHARACTERISTICS OF THE CEMENT

X-ray diffractometric analysis

The main component of almost all of the cements is a high-magnesian calcite (high-Mg calcite) close to 11 mol.% $MgCO_3$.

On average, low-magnesian calcite (low-Mg calcite) is ten times less abundant than high-Mg calcite (Fig. 11). This ratio is not related to the total carbonate content of the samples, which varies between 10% and 37% depending on the progress of growth in the pore space.

Low-Mg calcite is best represented in the samples from Fayté and Pierres de Sète. In the latter case, electron microprobe analysis shows increasing abundance of low-Mg calcite in the latest stages of cementation. Some magnesium-enriched calcite (18%, 28%, 36%, even 42%) can be detected in very low amounts in the samples from Saint-André, Tavac, Racou and Leucate, respectively, exceptionally reaching contents fairly close to the dolomitic end-member

(Fig. 11).

In summary, a comparison of the diffractograms of these cements leads to identification of several characteristics.

- The highest amounts of magnesium (>12 mol.% $MgCO_3$) are observed in Fayté and in the Leucate samples.
- Other high-Mg calcites have molar concentrations of $MgCO_3$ slightly lower or close to the lower limit accepted for these minerals (<5 mol.% $MgCO_3$).
- Low-Mg calcites were identified from Fayté and the Pierres de Sète but are less abundant than high-Mg calcite. In addition, X-ray microprobe analysis of some selected cements indicate that the MgO content ranges from 6.7 wt.% up to 9.1 wt.%. Although the volumes analyzed here are much smaller and may have a lower statistical value, these orders of magnitude are compatible with those inferred from diffractometric analysis.

Radiocarbon dating and stable isotope composition

Radiocarbon dating

Results are summarized in Table 2. They show consistent results, with ages decreasing with water depths.

Stable isotope composition

The stable isotope signatures of the eight analyzed cements indicate fairly homogeneous values; the data points are located respectively between +2‰ PDB and +4‰ PDB for $\delta^{18}O$ and between +1‰ PDB and +3‰ PDB for $\delta^{13}C$ (Fig. 12; Table 2). The Pierres de Sète cement shows an extreme value for both $\delta^{18}O$ and $\delta^{13}C$, but the data points remain very close to values for the inner shelf.

DISCUSSION

Mineralogical processes of cementation

Magnesian calcite is the main component (about 11 mol.% $MgCO_3$) of almost all samples, a value similar to cements already studied in the Mediterranean Basin (Alexandersson, 1969, 1972) and other low-temperature oceanic occurrences (Mackenzie *et al.*, 1983). The most important factor is temperature, and the magnesium concentration of calcite has been widely used to determine the temperature at which calcite precipitates (Mucci 1987; Oomori *et al.*, 1987; Burton & Walter, 1991).

Most of the studied beachrocks from the inner shelf show evidence for a single major episode of microcrystalline cementation (Fayté, Saint-André, Tavac and Racou). However, two samples (Pierres de Sète and Leucate 1) possibly record one or two subsequent stages of cementation that are more or less distinct.

1 An initial rapid cementation, observed in all the studied samples, records two or three stages of precipitation of micritic high-Mg calcite (including rare microsparites) as a coating around the grains, leading to an early stage of binding of sand and gravel particles (pore-lining). This early cement can invade almost the entire pore space, leaving only a few small voids for further crystallization (pore-filling).

2 A high-Mg calcite microsparitic cement resulting in the nearly complete filling of the remaining interstices, this stage represents only a small volume of cement.

3 A possible sparitic low-Mg calcite cementation can fill the last residual voids or is superimposed as an external envelope. It is thus a late process occurring in the presence of presumed brackish or

freshwater. In the case of the Pierres de Sète, the first micritic cementation was still incomplete before the precipitation of sparites.

Pore-lining and pore-filling have also been found to be common in various beachrocks (e.g. Aissaoui, 1988; Hird & Tucker, 1988; Scholle & Ulmer-Scholle, 2003). In the GoL beachrocks, the initial high-Mg micritic rims making up the second rim form a somewhat irregular coating around the grains. The high-Mg calcite crystals making up the second rim form a complete coating, suggesting that the sediment pore space was completely filled with water. Only the Pierres de Sète beachrock shows a distinct secondary fringe cement, composed of crystals growing into open pore spaces and characterized by acute terminations.

As in the case of the other beachrocks of the shelf, the Pierres de Sète were therefore located within the bathymetric range of the phreatic zone, thus allowing substantial horizontal water movement (Longman, 1980; Heckel, 1983; Neumeier *et al*., 2000). However, microscopic examinations of the GoL beachrocks do not reveal any microstalactitic or microfabric features characteristic of vadose-type cementation, such as meniscus cements or pendant cement under the grains as observed in Pleistocene beachrocks from Senegal (Giresse *et al.*, 1988; Diouf *et al*., 1995). Therefore the mixing of meteoric water and seawater cannot be evoked.

The Pierres de Sète beachrock represents a particular case because EDX analysis shows that the intensity of the Mg Kα peak displays a slight decrease or remains stable at a high position on the profiles. However, Mg-content variations in the same crystal are not accompanied by any change in crystal morphology. The crystal architecture is not modified when the early diagenetic environment evolves from marine to brackish. If there were a high meteoric groundwater table in the backshore area, then it would have been possible for low-Mg calcite cement to precipitate in the upper intertidal part of a beachrock. Commonly, marine waters may underlie or border the freshwater phreatic zone (Tucker & Wright, 1990). Therefore small oscillations in sea-level, causing subaerial exposure, can lead to the introduction of fresh or brackish water (Todd, 1988). Another explanation could be that there are differences between

the precipitation kinetics of high-Mg calcite and low-Mg calcite: the latter succeeding the former according to an increasing undersaturation of the pore waters.

Significance of isotopic values of calcitic cement

Considering the GoL $\delta^{18}O$ values as a whole, the data points characterize waters slightly colder than indicated by the usual oxygen isotope ratios of foraminifera and molluscs from coastal waters (in Tucker & Wright, 1990). However, the values are close to the field for carbonate cementation from the global marine environment (Andersson & Arthur, 1983; Holail & Rached, 1992) (Fig. 12).

The Pierres de Sète cement yields the highest positive values for both $\delta^{18}O$ and $\delta^{13}C$, but these values remain close to those from the inner shelf. This would reflect a slightly cooler water environment than for the other samples or suggests that the Pierres de Sète environment was isolated from dissolved carbon inputs of continental organic origin.

Are these cemented sediments beachrocks?

It could be argued that the lithified sands described here are not beachrocks *sensu stricto*, formed as beach or delta-front sediments lithified through the precipitation of carbonate cements (Vousdouskas *et al.,* 2007).

First of all, the morphology of these deposits clearly indicates that they follow palaeo-isobaths relative to periods of lower sea-level. Second, the coarse-grained texture is very similar to that of modern coastal deposits in the GoL. In the case of Pierres de Sète and Leucate, sedimentary structures (upper plane beds or large-scale cross beds) are also typical of coastal environments. All these arguments lead to the consideration that these deposits are real beachrocks and can thus be used as markers of past sea-level changes.

The coastal environment of the Gulf of Lions is only affected by very low (<30 cm) tidal

ranges that cannot be distinguished from oscillations induced by storms or changes in barometric pressure. As a result, there is no intertidal zone and therefore the characteristic hydrology of this zone (vadose water, phreatic water) cannot be found here.

Biomediation can be the main factor in the formation of tropical beachrocks (McCutcheon *et al.*, 2016). Because there was no observation of any subtidal cryptic microbialites trapping and bounding detrital material, this hypothesis was excluded.

Position of the Pierres de Sète samples, a puzzling problem

Two radiocarbon ages were obtained by Mauffrey *et al*. (2015), from the upper and lower parts of the sample (10 cm apart). These dates were calibrated with the new version of Calib8.2 (Table 2). Because the precise position of the sample was not determined, only the overall navigation track of the dredge being known (Fig. 3), previous authors initially assumed that the cementation took place at the top of the barrier (90 m). This remains a matter for speculation as long as there are no available *in situ* observations or other samples (with a remotely operated vehicle – ROV). It may be that these beachrocks were situated deeper than initially suggested, somewhere between 100 m and 90 m, and were eventually encrusted by bioherms. Such bioconstructions, which are termed coralligenous in the Mediterranean Sea (Ballesteros 2006), may form banks up to 4 m thick, possibly entirely covering the beachrocks. This hypothesis is supported by the fact that encrusted fragments of dead corals (*Dendrophyllia cornigera*) and calcareous algae (*Lithothamnium sp.*) were found in the dredge. Without definitive answer to these questions, a very conservative total vertical error of ±5 m was applied to these two samples, corresponding to the sum of positioning error and indicative range.

Depositional environments of the Gulf of Lions beachrocks

Local versus elongated beachrock barriers

In the western Mediterranean, beachrock exposures are relatively rare and are most often located in shallow environments near the present-day coast, and evidence of greater water

depth is only rarely recognized (Vacchi *et al*., 2016). They have so far never been described in detail in the case of the Gulf of Lions.

As mentioned in Mauz *et al*. (2015), the zone of recent beachrock formation is restricted to coastal environments with low sedimentation rates, relatively flat morphology and warm sea-surface temperature. At each site, the lithified sedimentary body is indeed formed on the foreshore immediately seaward of the shoreline. Mauz *et al*. (2015) considered that a beachrock deposit is not a continuous body, but an area restricted in time and space. However, several examples from the GoL show alignments with a lateral extent of several hundred metres to kilometres. Similar elongated barriers are described along the western Sardinian margin at depths (15 to 30 m) similar to the inner shelf GoL beachrocks (de Falco *et al.*, 2015). In fact, the Pierres de Sète provides an example where both isolated pinnacles and elongated barriers are observed. It is likely resulting from differential erosion, where the less consolidated intervals have been eroded, as observed in the recent coastal Leucate beachrocks.

Asymmetry of the barriers

The morphology of most beachrock barriers on the GoL shelf shows a marked asymmetry with a steeper slope on the seaward than on the landward flank. In other Mediterranean barriers, it has already been noted that the landward flank generally shows less developed cementation (e.g. Russell, 1959; Alexandersson, 1969), which may suggest that the cementation process may be longer (or faster) on the seaward side under the action of swell. In any event, under constant hydrodynamic conditions, the landward part of beachrock beds is better preserved, while its seaward part is more likely to be reworked by wave energy. Therefore, the asymmetric morphology of the barrier could be controlled by differential erosion. Along the Leucate beach, the exposure of beachrocks protects the beach against erosion and causes wave dissipation which reduces the erosive effects of wave energy on the shore (Aleman *et al.,* 2011).

Doubled barriers

The succession of two parallel lithified barriers observed in this study at several locations (Pierres de Sète, Racou, Leucate and Tavac) can be interpreted in terms of a succession of phases of barrier cementation and overstepping in a context of slow sea-level rise, as proposed for the south Florida margin (Locker *et al*., 1996) or the west margin of Sardinia (de Falco *et al.,* 2015). In the latter case, up to five parallel ridges were described by these authors.

Implication for sea-level variations in the Gulf of Lions

This study's results are insufficient to establish a local sea-level curve for the post-LGM sea-level rise, but they do provide new information for certain time frames that are so far poorly known. They can also be compared to previous sea-level curves proposed for this area, as well as to studies from other areas worldwide, provided that subsidence *s.l.* is considered (Fig. 13).

Comparison with other local past sea-level estimates

Surprisingly, the best fit between the results of this study and previous studies in the GoL is found in the earliest work of Labeyrie *et al.* (1976) (green dotted line in Fig. 13). Present results agree with other studies for the upper Holocene (4.2 to 0 ka BP), but they show a shift (deeper values for equivalent ages) comprised between 10 m and 20 m for the lower Holocene and middle Holocene (11.7 to 4.2 ka BP). The highest differences are reached for the 7 to 5 ka time interval, but the positive palaeo-sea-levels (up to +4m) found by Aloïsi (1986) are considered as unlikely for the Holocene French Mediterranean coastline (Lambeck & Bard, 2000). The comparison of the study's data with the more recent results of Vacchi *et al.* (2016) and Salel *et al.* (2020) also indicate, for the middle Holocene, a shift in the order of 10 to 15 m in the same direction. In the case of Vacchi *et al.* (2016), most of the sea-level index points (SLIP) are from the Rhône delta, a zone with a different tectonic regime compared to the western Gulf of Lions (Vella & Provensal, 2000), but this cannot explain the magnitude of the observed differences.

Comparison with predicted relative sea-level curve for the western Gulf of Lions (central shelf) and other data

A comparison with sites from different locations requires that the averaged global sea-level be corrected from the subsidence history of the margin. For this purpose, the global ice equivalent sea-level curve of Lambeck *et al.* (2014), based on more than 1000 observations in the far field was used. Local corrections (for the central continental shelf of the western Gulf of Lions) due to tectonic/thermal subsidence and sediment and water loading, as determined by Jouet *et al.* (2008) were applied to this curve. These authors applied the *Sedflux* (Hutton & Syvitski, 2008) forward stratigraphic model to determine the various components of subsidence, including the hydro-isostatic load. Results show that for the last *ca* 10 kyr (the Holocene), the relative sea-level in the study area is almost identical to the global one. On the other hand, Jouet *et al.* (2008) showed that the outer shelf subsided by about 20 m under the effect of total subsidence since the Last Glacial Maximum (*ca* 20 ka BP). Based on their results, we created a composite relative sea-level curve for the western Gulf of Lions central shelf (red solid line in Fig. 13).

Except for the oldest and recent most beachrocks (sites 1 and 6–7, respectively), that fit the prediction within the error bars, the current results present a systematic shift compared to the predicted sea-level, suggesting that either the ^{14}C dates are too young, or that palaeo-depths are overestimated. In the first scenario, a possible explanation might be that a second phase of cementation occurred after deposition. It is shown however, that such secondary cementation was not observed on the dated samples. As to an error on the initial position of the samples, it also seems unlikely to explain the difference between predicted and measured sea-levels, ranging from 8 m (Racou, 5 in Fig. 13) to 18 m (Saint André, 3 in Fig. 13). These differences would imply that a thick prism of coastal deposits, partly lithified, was eroded by the action of waves, but the observed morphology of these deposits rather suggests a good preservation of initial topography. In any event, when important erosion occurs, like in the case of Pierres de Sète, the beachrock remain at (or in the vicinity of) their initial position, forming important pinnacles all over the outer shelf. Interestingly, the palaeo-sea-levels of Berné *et al.* (2007), obtained by a completely different method, also display a shift in the order of 8 m between predicted and estimated sea-levels.

At this stage, there is no robust answer to these puzzling questions. Only precise mapping and sampling using Remote or Autonomous Underwater Vehicles might allow determining, if possible, the initial conditions of formation of these beachrocks.

CONCLUSIONS

During the last sea-level rise (last *ca* 20 kyr), temperature and sunshine conditions have favoured in the Gulf of Lions the precipitation of high-magnesian calcite (high-Mg calcite), which led indifferently to the cementation of sands, gravels and pebbles. The surface of the continental shelf displays several irregularities in relief making up more or less continuous barriers extending over several hundred or several thousand metres. They are foreshore deposits formed in less than 1 m water depth, strictly corresponding to the definition of beachrocks. Subsequently they were subject to differential erosion, rising from the surrounding sea floor by up to 1 to 3 m, exceptionally up to 20 m on the outer shelf.

The recurrence of these barriers in space allows for data points at several depths never investigated by previous studies to be provided. Barriers fossilized by cementation are more abundant towards the outer edge (around -90 m) and between -25 m and -10 m, probably in relation with a lower rate of sea-level rise. It can be noted that several of these barriers form double ridges (Pierres de Sète, Tavac, Leucate) possibly in relation with a period of stillstand in sea-level rise.

Unlike certain confined waters of the eastern Mediterranean, where rare aragonite precipitation is observed, the cement of beachrock sandstones in the Gulf of Lions is made up almost entirely of calcite. These cements are formed by rapid precipitation of micrites, which initially provide most of the binding phase; later, high-Mg calcite sparites may be deposited in the remaining voids. Sometimes, supersaturation at the water surface can be disturbed by irregularities in the swell pattern, which interrupt the cementation of the sandy body. Finally, a late-stage deposit of low-magnesian calcites (low-Mg calcite) may be associated with the local

input of brackish water, such as in the Pierres de Sète. The isotopic compositions of GoL beachrock cements are close to predictions made from carbon and oxygen fractionation equations for abiogenic precipitation at a given temperature and pressure. Coastal- and outer shelf-samples provide sea-level index points in agreement with previous studies and with predicted sea-level using Ice equivalent sea-level. However, inner shelf samples display a shift ranging from 8 to 18 m with predicted sea-level (the observed water depths being deeper than the predicted ones). This shift has not been explained so far and remains a source of future research, especially for the deposits found around -90 m water depth.

ACKNOWLEDGEMENTS

Acquisition of data at sea benefited from the dedication of crews and technical teams of IFREMER/GENAVIR aboard *R/V "l'Europe*" and *"L'Haliotis"*. Radiocarbon ages were obtained through the ARTEMIS National French Programme. The members of the LMC14 team (Lucile Beck, Emmanuelle Delke-Količ, Jean-Pascal Dumoulin and Christophe Moreau) are thanked for assistance during the entire process. Fabien Dewilde (CNRS-IUEM Brest) is thanked for Oxygen and Carbon isotope analyses, as well as Christophe Menniti (Université de Perpignan, CEFREM) for Total Organic Carbon analysis. Helmut Zibrovius (Centre d'Océanologie de Marseille) determined the dredged coral samples. Michael Carpenter post-edited the English style and grammar. We thank John Reijmer, Eberhard Gischler, Gregor Eberli and Peir Pufahl, Editor-in-Chief, *Sedimentology*, and two anonymous reviewers for their thorough reading that greatly improved the manuscript. This paper is dedicated to the memory of Paolo Pirazzoli, a fine and acknowledged connoisseur of Quaternary Mediterranean shorelines.

DATA AVAILABILITY

The data that support the findings of this study are available from the corresponding author upon reasonable request.

REFERENCES

Aissaoui, D.M. (1988) Magnesian calcite cements and their diagenesis: dissolution and dolomitization, Muruora Atoll. *Sedimentology*, **35**, 821-841.

Aleman, N., Robin, N., Certain, R., Vanroye, C., Barusseau, J.P., Bouchette, F. (2011). Typology of nearshore bars in the Gulf of Lions (France) using LIDAR technology. *Journal of Coastal Research,* **64**, 721-725.

Alexandersson, T. (1969) Recent littoral and sublittoral high-Mg calcite lithification in the Mediterranean. *Sedimentology,* **12**, 47–61.

Alexandersson, T. (1972) Mediterranean beachrock cementation: marine precipitation of Mg calcite. In: *The Mediterranean Sea: a natural sedimentation laboratory* (Ed. D.J. Stanley), pp. 203-223, Dowden, Hutchinson and Ross, Inc., Strousburg.

Aloïsi, J. C., Monaco, A., Thommeret, J. and Thommeret, Y. (1975). Evolution paléogéographique du plateau continental languedocien dans le cadre du Golfe du Lion. Analyse comparée des données sismiques, sédimentologiques et radiométriques concernant le Quaternaire récent. *Revue de Géologie Dynamique et de Géographie Physique* **17**(1): 13-22.

Aloïsi, J. C. (1986). Sur un modèle de sédimentation deltaïque: contribution à la connaissance des marges passives. *Unpublished PhD Thesis*, Perpignan University, 162 pp.

Aloïsi, J.C., Monaco, A., Planchais, N., Thommeret, J., Thommeret, Y. (1978) The Holocene transgression in the Golfe du Lion: paleogeographic and paleobotanical evolution. *Géogr. Phys. et Quat.*, **XXXII** (2), 45-162.

Amorosi A., Rossi V., Sarti, G., Matei, R. (2013) Coalescent valley fills from the late Quaternary record of Tuscany (Italy). Quaternary International, **288** 129-138.

Anderson, T.F., Arthur, M.A. (1983) Stable isotopes of oxygen and carbon and their application to sedimentologic and paleoenvironmental problems. In: *Stable Isotopes in Sedimentary Geology*, Eds. M.A. Arthur and T.F. Anderson*, Soc. Econ. Paleont. Miner.* Short course, **10**, 1.1-1.151.

Ballesteros, E. (2006) Mediterranean coralligenous assemblages: a synthesis of present knowledge. In: *Oceanography and Biology: an annual review* (Eds R. N. Gibson, R. J. A. Atkinson and J. D. M. Gordon. Boca raton, Taylor & Francis. **44,** 123-195.

Bard, E., Hamelin, B., Arnold, M., Montaggioni, L., Cabioch, G., Faure, G., Rougerie, F. (1996) Deglacial sea-level record from Tahiti corals and the timing of global meltwater discharge. *Nature,* **382**, 241–244.

Bassetti, M.A., Berné, S., Jouet, G., Taviani, M., Dennielou, B., Flores, J.A., Gaillot, A., Gelfort, R., Lafuerza, S., Sultan, N. (2008) The 100-ka and rapid sea level changes recorded by prograding shelf sand bodies in the Gulf of Lions (western Mediterranean Sea). *Geochem. Geophys. Geosyst.* **9** (11). http://dx.doi.org/10.1029/2007GC001854/.

Berné, S., Lericolais, G., Marsset, T., Bourillet, J.F., De Bastit, M. (1998) Erosional shelf sand ridges and lowstand shorefaces: examples from tide and wave dominated environments of France. *J. Sedim. Res*., **68(4),** 540-555**.**

Bourcart J. (1945) Étude des sédiments pliocènes et quaternaires du Roussillon. *Bull. Serv. Carte géol. France,* **45**, 395-476.

Burton, E.A., Walter, L.M. (1991) The effects of P_{CO2} and temperature on magnesium incorporation in calcite in sea water and $MgCl_2$ – $CaCl_2$ solution. *Geoch. and Cosmochemica* Acta, **55**, 777-785.

Catuneanu, O. (2019) Model-independent sequence stratigraphy. *Earth-Science Reviews*, **188,** 312-388.

De Falco, G., Antonioli, F., Fontolan, G., Lo Presti, V., Simeone, S. and Tonielli, R. (2015) Early cementation and accommodation space dictate the evolution of an overstepping barrier system during the Holocene. *Marine Geology*, **369,** 52-66.

Desruelles S., Fouache E., Ciner A., Dalongeville R., Pavlopoulos K., Kosun E., Coquinot Y., Potdevin J.-L. (2009) Beachrocks and sea level changes since Middle Holocene: Comparison between the insular group of Mykonos-Delos-Rhenia (Cyclades, Greece) and the southern coast of Turkey. *Global Planetary Change,* **66**, 1-2, 19-33.

Diouf, B., Giresse, P., Occhietti, S., Causse, C. and Pichet, P. (1995) A petrological and geochemical study of the calcareous sandstone of West African marine Pleistocene (Cap des Biches, Senegal). *Quat. Intern.*, **29/30**, 49-60.

Dumoulin, J. P., C. Comby-Zerbino, E. Delqué-Količ, C. Moreau, I. Caffy, S. Hain, M. Perron, B. Thellier, V. Setti, B. Berthier, L. Beck L. (2017) "Status Report on Sample Preparation Protocols Developed at the LMC14 Laboratory, Saclay, France: From Sample Collection to 14C AMS Measurement." *Radiocarbon*, **59**(3), 713-726.

Fahad, M., Saeed, S. (2018) Determination and estimation of magnesium content in the single phase magnesium-calcite [$Ca_{(1-x)}Mg_xCO_{3(s)}$] using electron probe microanalysis EPMA and X-ray diffraction (R.X). *Geosc. J.,* 10 p. http://dx.doi.org/10.1007/s12303-017-0059-8

Falkenroth, M., Schneider, B., Hoffmann, G. (2019) Beachrock as sea-level indicator - a case study at the coastline of Oman (Indian Ocean). *Quat. Sci. Rev*. **206**, 81-98

Fanget, A.-S., Bassetti, M.A., Arnaud, M., Chiffoleau, J.F., Cossa, D., Goineau, A., Fontanier, C., Buscail, R., Jouet, G., Maillet, G.M. (2013) Historical evolution and extreme climate events during the last 400 years on the Rhône prodelta (NW Mediterranean*). Mar. Geol*. **346**, 375-391.

Giresse, P., Diouf, M., Barusseau, J.-P. (1988) Lithological, mineralogical, and geochemical observations of Senegalo-Mauritanian Quaternary shorelines deposits: possible chrononological revisions. *Palaeogeogr., Palaeoclimatol., Palaeoecol.,* **68**, 241-257.

Goldsmith, J.R., Graf, D.L., Heard, H.C. (1961) Lattice constants of the calcium-magnesium carbonates. *American Mineralogist,* **46**, 453–457.

Got, H., Aloisi, J.C. (1990) The Holocene sedimentation on the Gulf of Lions margin: a quantitative approach. *Cont. Shelf Res.,* **9-11**, 841–855.

Guieu, C., Martin, J.M., Thomas, A.J., Elbaz-Poulichet, F. (1991) Atmospheric versus river inputs of metals to the Gulf of Lions. Total concentrations, partitioning and fluxes. *Mar. Pollut. Bull*., **22** (4), 176–183.

Hird, K., Tucker, M.E. (1988) Contrasting diagenesis of two Carboniferous oolites from South Wales: a tale of climatic influence. *Sedimentology*, **35**, 587-602.

Holail, H., Rashed, M. (1992) Stable isotopic composition of carbonate-cemented recent beachrock along the Mediterranean and the Red Sea coasts of Egypt. *Mar. Geol*., **106**, 141–148.

Hutton, E. W. H., Syvitski, J.P.M. (2008). Sedflux 2.0: An advanced process-response model that generates three-dimensional stratigraphy. *Computers & Geosciences* **34**: 1319-1337.

Jouet, G., Berné, S., Rabineau., M., Bassetti, M.A., Bernier, P., Dennielou, B., Sierro, F.J., Flores, J.A., Taviani, M. (2006) Shoreface migrations at the shelf edge and sea level changes around the Last Glacial Maximum (Gulf of Lions, NW Mediterranean). *Mar. Geol.,* **234** (1–4), 21–42. http://dx.doi.org/10.1016/j.margeo.2006.09.012.

Jouet, G., Hutton, E. W. H. , Syvitski, J. P. M., and Berné, S. (2008). Response of the Rhône deltaic margin to loading and subsidence during the last climatic cycle. *Computers & Geosciences* **34**: 1338-1357.

Labeyrie, J., Lalou, C., Monaco, A., Thommeret, J. (1976) "Chronologie des niveaux eustatiques sur la côte du Roussillon de -33000 ans B.P. à nos jours." *Comptes Rendus Acad. Sci. Paris*, **282**, 349-352.

Lambeck, K. and Bard, E. (2000). Sea-level change along the French Mediterranean coast for the past 30 000 years. *Earth and Planetary Science Letters* **175**: 203-222.

Lambeck, K., Rouby, H., Purcell, A., Sun, Y., Sambridge, M. (2014). Sea level and global ice volumes from the Last Glacial Maximum. *Proceedings of the National Academy of Sciences* **111**(43): 15296-15303.

Locker, S.D., Hine, A.C., Tedesco, L.P., Shinn, E.A. (1996) Magnitude and timing of episodic sea-level rise during the last deglaciation. *Geology*, **24,** 827-830.

Longman, M.W. (1980) Carbonate diagenetic textures from nearsurface diagenetic environments. *Bull.AAPG.,* **64**(4), 461-487.

Mackenzie, F.T., Bischoff, W.D., Bishop, F.C., Loijens, M., Schoonmaker, J., Wollast, R. (1983) Magnesian calcites: low-temperature occurrence, solubility and solid solution behaviour. In: *Carbonates: Mineralogy and Chemistry*. *Rev. of Mineral.*, **11**, 97-144.

Mauffrey, M.A., Berné, S., Jouet, G., Giresse, P., Gaudin, M. (2015) Sea-level control on the connection between shelf-edge deltas and the Bourcart canyon head (western Mediterranean) during the last glacial/interglacial cycle. *Mar. Geol.*, **370**, 1–19.

Mauz B., Vacchi M., Green, A, Hoffmann, G., Andrew Cooper, A. (2015) Beachrock: a tool for reconstructing relative sea level in the far-field. *Mar. Geol.*, **362**, 1-16.

McCutcheon, J., Nothdurft, L., Webb, G.E., Paterson, D., Southam, G. (2016) Beachrock formation via microbial dissolution and re-precipitation of carbonate minerals. *Mar. Geol.*, doi: 10.1016/j.margeo.2016.10.010

Millot, C.A. (1990) The Gulf of Lions'hydrodynamic. *Cont. Shelf Res*., **9–11**, 885–894.

Moreau, C., Messager, C., Berthier, B., Hain, S., Thellier, B., Dumoulin, J.-P., Caffy, I., Sieudat, M., Delqué-Količ, E., S. Mussard, S., Perron, M., Setti, V., Beck, L. (2020) "Artemis", the ^{14}C AMS facility of the LMC A4 national laboratory: a status report on quality control and microsample procedures. *Radiocarbon,* **62(6),** 1755-1770.

Neumeier, U., Bernier, P., Dalongeville, R., Oberlin, C. (2000) Les variations holocènes du niveau marin mises en évidence par les caractères et la diagenèse des beachrocks: exemple de Damnoni (Crète). *Géomorphologie : relief, processus, environnement,* **4**, 211-220.

Oomori, T., Kaneshima, H., Maezato, Y., Kitano, Y. (1987) Distribution coefficient of Mg^{2+} ions between calcite and solution at 10-50°C. *Marine Chem*., **20**, 327-336.

Pirazzoli, P.O., Tomasin, T., Ullmann, A. (2007) Extreme sea levels in two northern Mediterranean areas, Risques littoraux en Méditerranée. *J. Medit. Geogr.*, **108**, 59-68. https://doi.org/10.4000/mediterranee.170

Rabineau, M. (2001) Un modèle géométrique et stratigraphique des séquences de dépôts : enregistrement des cycles climatiques de 100, 000 ans. *Unpublished PhD Thesis*, Rennes I University, 445 pp.

Rabineau, M., Berné, S., Aslanian, D., Olivet, J.-L., Joseph, P., Guillocheau, F., Bourillet, J.-F., Ledrezen, E., Granjeon, D. (2005) Sedimentary sequences in the Gulf of Lion: A record of 100,000 years climatic cycles. *Mar. Pet. Geol.,* **22** (6–7), 775–804. http://dx.doi.org/10.1016/j.marpetgeo.2005.03.010

Rabineau, M., Berné, S., Olivet, J.L., Aslanian, D., Guillocheau, F., Joseph, P. (2006) Paleo sea levels reconsidered from direct observation of paleoshoreline position during Glacial Maxima (for the last 500,000 yr). *Earth and Planetary Science Letters* **252** (1-2): 119-137.

Rabineau, M., Leroux, E., Aslanian, D., Bache, F., Gorini, C., Moulin, M., Molliex, S., Droz, L., dos Reis, A.T., Rubino, J.L., Guillocheau, F. and Olivet, J.L. (2014) Quantifying subsidence and isostatic readjustment using sedimentary paleomarkers, example from the Gulf of Lion. *Earth and Planetary Science Letters*, **388,** 353-366.**Ramsay, P.J., Cooper, J.A.G.** (2002) Late Quaternary sea-level change in South Africa. *Quaternary Research,* **57**, 82-90.

Rovere, A., Stocchi, P., Vacchi, M. (2016) Eustatic and Relative Sea Level Changes Current Interglacials and relative sea-level highstands Climate Change Reports 2(4) DOI: 10.1007/s40641-016-0045-7

Russell, R.J. (1959) Caribbean beach rock observation. Z. *Geomorphol*., **3**, 227–236.

Salel, T., C. Flaux, H. Bruneton, P. Degeai, B. Debvillers, Lefevre, D. (2020) Changements du niveau marin relatif à l'Holocène ancien et moyen sur la côte du golfe du Lion (in French with English abstract).*Quaternaire,* **31**(1), 33-44.

Scholle, P.A., Ulmer-Scholle, D.S. (2003) A color guide to the petrography of carbonate rocks: grains, textures, porosity, diagenesis. *AAPG*, Tulsa, Oklahoma, 474 pp.

Shackleton, N.J. (1987) Oxygen isotopes, ice volume and sea level. *Quaternary Science Reviews*, **6,** 183-190.

Shennan, I., Horton, B. (2002) Holocene Land- and sea-level changes in Great Britain. *Journal of Quaternary Science*, **17,** 511-526

Siani, G., Paterne, M., Arnold, M., Bard, E., Métivier, B., Tisnerat, N., & Bassinot, F. (2000). Radiocarbon Reservoir Ages in the Mediterranean Sea and Black Sea. *Radiocarbon, **42*** (2), 271-280.

Siddall, M., E. Rohling, A. Almogi-Labin, C. Hemleben, D. Meischner, I. Schmelzer, Smeed, D.A. (2003) Sea-level fluctuations during the last glacial cycle. *Nature*, **423**, 853-858.

Stuiver, M., Reimer, P.J. (1993) Extended ^{14}C database and revised CALIB radiocarbon calibration program. *Radiocarbon,* **35**, 215–230.

Todd, D.K. (1988) *Groundwater hydrology*. John Wiley & Sons, London, 535 pp.

Tucker, M.E., Wright, **V.P.** (1990) *Carbonate sedimentology*. Blackwell Scientific publications, 482 pp.

Vacchi, M., Marriner, N., Morhange, C., Spada, G., Fontana, A.,Rovere, A. (2016) Multiproxy assessment of Holocene relative sea-level changes in the western Mediterranean: Sea-level variability and improvements in the definition of the isostatic signal. *Earth-Sci. Rev.*, **155**, 172–197.

Vella, C., Provansal, M. (2000) Relative sea-level rise and neotectonic events during the last 6500 yr on the southern eastern Rhône delta, France. *Mar. Geol.,* **170**(1-2): 27-39.

Vousdoukas, M.I., Velegrakis, A.F., Plomaritis, T.A. (2007) Beachrock occurrence, characteristics, formation mechanisms and impacts. *Earth-Sci. Rev.,* **85**, 23–46.

Waelbroeck, C., Labeyrie, L., Michel, E., Duplessy, J.C., McManus, J.F., Lambeck, K., Balbon, E., Labracherie, M..–(2002) Sea-level and deep water temperature changes derived from benthic foraminifera isotopic records. *Quaternary Science Reviews*, **21,** 295-305.

FIGURE AND TABLE CAPTIONS

Fig. 1. Location of studied sites in the Gulf of Lions. 1: 'Pierres de Sète'; 2 to 5: inner shelf samples; 6–7: Leucate coastal barriers. Isobaths are at every 5 m between 0 m and 150 m, and every 50 m beyond 150 m.

Fig. 2. Stages of separation of calcitic crystals from cement. (**A**) After a first grinding, composite aggregates of detrital and biogenic grains still cemented (bio: bioclasts, Q: quartz, yellow arrows: micrite cement). (**B**) After a second grinding and selection, light and dark micrite or microsparite cement debris intended for AMS dating.

Fig. 3. Swath bathymetric map (SIMRAD EM1000) of the 'Pierres de Sète' area. This relief is located near the shelf edge, near the Bourcart canyon head. The dotted line represents the seaward limit of offshore sands. The two solid black lines (CLDr01) represent the track of the dredging operation. The red line corresponds to the seismic profile (BAS 05) presented in Fig.4.

Fig. 4. Seismic profile BAS 05 across the Pierres de Sète (position in Fig. 3). The Pierres de Sète barrier is situated on top of large sand bodies deposited during the sea-level fall between Marine Isotope Stages MIS 3 and MIS 2 (Jouet *et al.*, 2006; Bassetti *et al.,* 2008). The identification of seismic surfaces and units is based on information from borehole PRGL2.2, situated 2.5 km to the north-east, benefitting from the very dense grid of seismic profiles in the area (see Bassetti *et al.*, 2008 for details). MRS: maximum regressive surface in the sense of Catuneanu (2019). The yellow pattern corresponds to sand and the green pattern to clay/silt-dominated deposits, based on borehole information and seismic facies. The seaward limit of offshore sands is situated about 1 km further to the south-east.

Fig. 5. Swath bathymetric and acoustic maps of three inner shelf barriers. (**A**) Fayté. (**B**) Saint-André. (**C**) Tavac (black star: sampling location).

Fig. 6. Swath bathymetric map and vertical profiles across the two successive Racou barriers near Precambrian basement outcrops. Cross-sections 1 and 2 highlight the change in symmetry and relief along the barriers.

Fig. 7. Satellite image (Google Earth) of successive barriers seaward of Leucate beach. Cross-section A to B. Reconstructed location of beachrock outcrops on Leucate beach (during low tide 0.4 m). L1 indicates the position of sample Leucate 1. L2 is situated slightly further north, along the same alignment. The beachrock lithification is suggested to occur at *ca* - 0.35 m (NGF-IGN69: altimetric system of continental France).

Fig. 8. Macroscopic facies. (**A**) Surface section of Pierres de Sète with crossed stratification. (**B**) Roches de Fayté. (**C**) Tavac; puddingstone structure. (**D**) Racou. (**E**). Leucate 1, strongly cemented beachrock outcropping in long continuous banks. (**F**) Leucate 2, lateral passage to a facies of incompletely cemented beachrocks blocks, easily crushed by hand. Q; quartz, S: schist, G: gneiss pebble, sc: sandstone clast.

Fig. 9. Beachrock microfacies (plane polarized light). (**A**) Pierres de Sète; quartz, bioclasts and an extraclast are surrounded by complete rims of high-Mg calcite cement with palisade-type fabric. (**B**) Fayté; poorly sorted grains (fine and coarse sand) in the micritic cement. (**C**) Saint-André; high-Mg calcite with microsparitic crystals in the rectangle representing an exception. (**D**) Racou; homogeneous micritic cement over the entire surface of the rock.

Fig. 10. Scanning electron microscopy (SEM) images. (**A**) Pierres de Sète; siliciclastic grains are completely surrounded by magnesian calcite crystals of prismatic shape, 5 to 10 µm long (palisade fabric with crystalline-continuous calcitic growth). Sometimes, these crystals are preceded by a coating of micritic crystals, 1 to 2 µm long. (**B**) Pierres de Sète; the prismatic rhomb shape of euhedral to anhedral crystals corresponds to c-axis growth, parallel to the apex of the rhombohedron crystals. (**C**) Tavac; successive micrite and microsparite accumulations (yellow arrows) on angular quartz grain (Q). (**D**) Racou; slightly degraded apical ends of palisade high-Mg calcite crystals.

Fig. 11. Chemical composition of calcites from cements of different beachrocks; the intensity of each X-ray diffraction peak was evaluated by data processing (Leucate 1: complete cementation, Leucate 2: incomplete cementation)

Fig. 12. Stable isotope signatures of Gulf of Lions (GoL) beachrock cement. The samples (1 to 7) are located in Fig. 1

Fig. 13. Relative sea-levels inferred from beachrocks in the Gulf of Lions (GoL) (red rectangles) and comparison with other local data sets. Numbers in red refer to Sea-Level Index Points positioned in Fig. 1. For each rectangle, the horizontal is the 2 sigma error on the calibrated age, and the vertical is the sum of errors (including the indicative range) on the elevation. See explanation in the *Methods* section. The red curve is the global ice equivalent sea-level of Lambeck *et al.,* (2014), modified for taking into account the subsidence history of the central western Gulf of Lions (see explanation in text).

Table 1. Morphological characteristics of the lithified sand barriers of the Gulf of Lions (GoL). *Relief* corresponds to the maximum elevation with respect to the surrounding seafloor.

Table 2. Characteristics, radiocarbon ages, oxygen and carbon isotopic values of selected calcite crystals in beachrock cements from the Gulf of Lions (GoL) shelf. The Marine20 curve of the CALIB 8.2 calibration programme (Stuiver *et al.*, 2020) was used, where the modern global ocean age is now modelled at 550 years instead of 400 years. The averaged regional marine radiocarbon reservoir age correction ΔR of -43 and an averaged uncertainty of 45 for the Marine 20 calibration, based on Siani *et al.* (2000) was also used. The same corrections are applied to the ^{14}C ages of samples already studied/published. The estimate on the vertical error for each sample is explained in the *Methods* section.

Location	Site name and number	Water depth (m)	Relief (m)	Length (m)	Width (m)	Double barrier
Outer shelf	Pierres de Sète (1)	10–90	18	>10,000	300	x
Inner shelf	Fayté rocks (2)	25	2	1470	20–40	x
Inner shelf	Saint André rocks (3)	25	1	100	30	
Inner shelf	Tavac rocks (4)	20	3	880	30–50	x
Inner shelf	Racou rocks (5)	10	1.5	375	40	x
Inner shelf	Racou rocks	12	2	200	30	x
Present beach	Leucate 1 (6)	0.35	0.5	>10,000	20	x
Present beach	Leucate 2 (7)	0.35	0.5	>10,000	20	x

Sea-level index point	Location	Lat. N. (°)	Long. E (°)	Water depth (m)	Vertical error (±m)	Lab. number	Radiocarbon age (a BP)	Error age (±a BP)	2 σ Calibrated age (a BP)	Median probablity (a BP)	$\delta^{13}C/^{12}C$ vs v. PDB	$\delta^{18}O/^{16}O$ vs v. PDB
1a	P. de Sète-upper	42.815	3.628	95	5	Poz-42577	15,110	80	17,197–17,870	17,530	–	–
1b	P. de Sète-lower	–	–	95	5	Poz-42578	16,050	90	18,260–18,839	18,583	–	–
2	Fayté	42.539	3.092	25	2	SacA-60059	7540	30	7686–8011	7860	+2.69	+1.77
3	St André	42.563	3.082	23	2	SacA-60060	6470	30	6595–6988	6788	+2.24	+2.11
4	Tavac	42.552	3.072	20	2	SacA-60469	6045	35	6139–6507	6321	+1.09	+1.56
5	Racou	42.540	3.059	10	2	SacA-60062	5200	30	5251–5586	5415	+1.05	+1.17
6	Leucate 1	42.888	3.0334	0.35	1.5	SacA-60063	1190	30	502–774	633	+2.68	+2.12
7	Leucate 2	42.900	3.059	0.35	1.5	SacA-60064	4250	30	4001–4418	4222	+2.83	+1.90

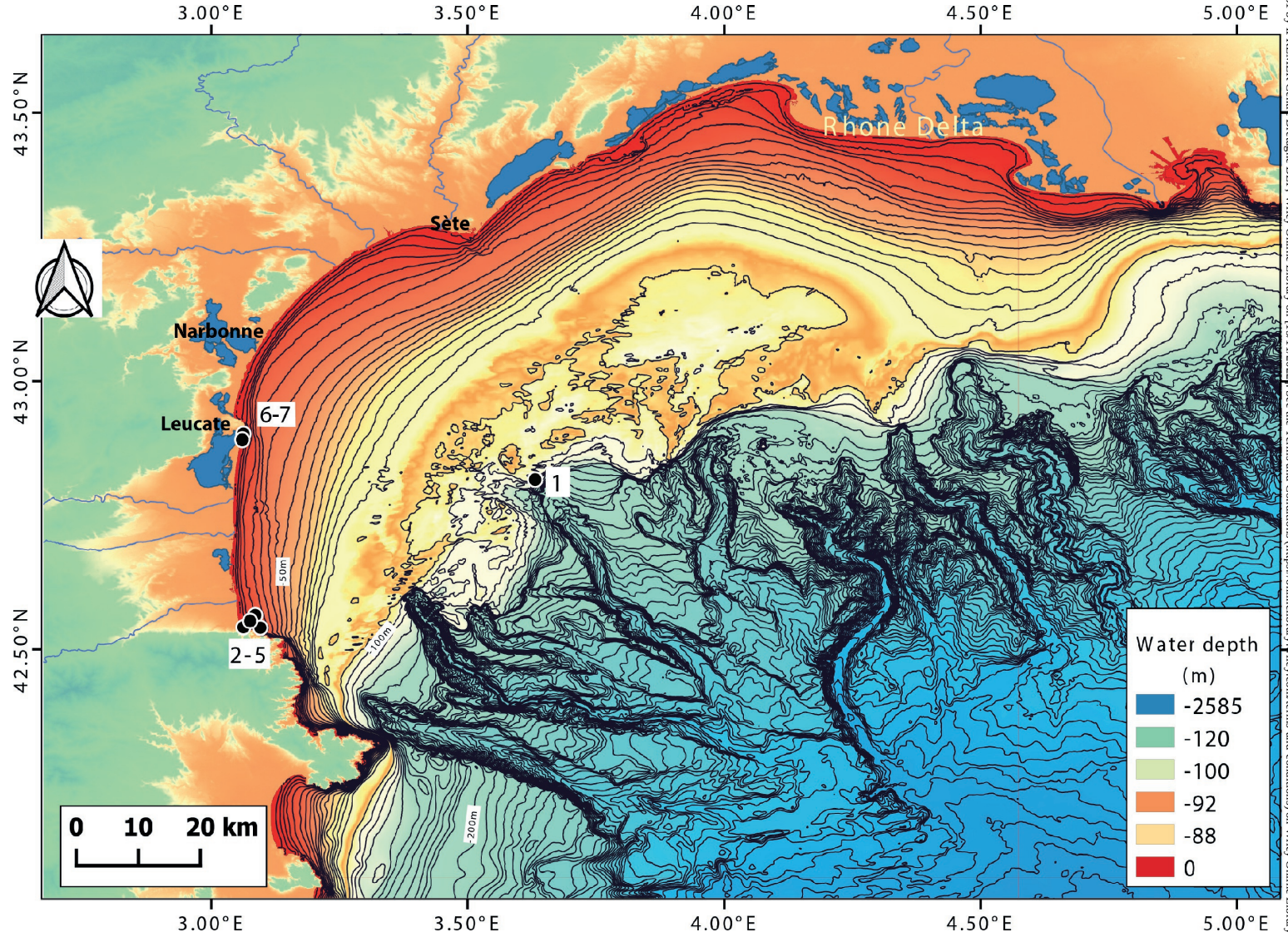

sed_13061_fig. 1.eps

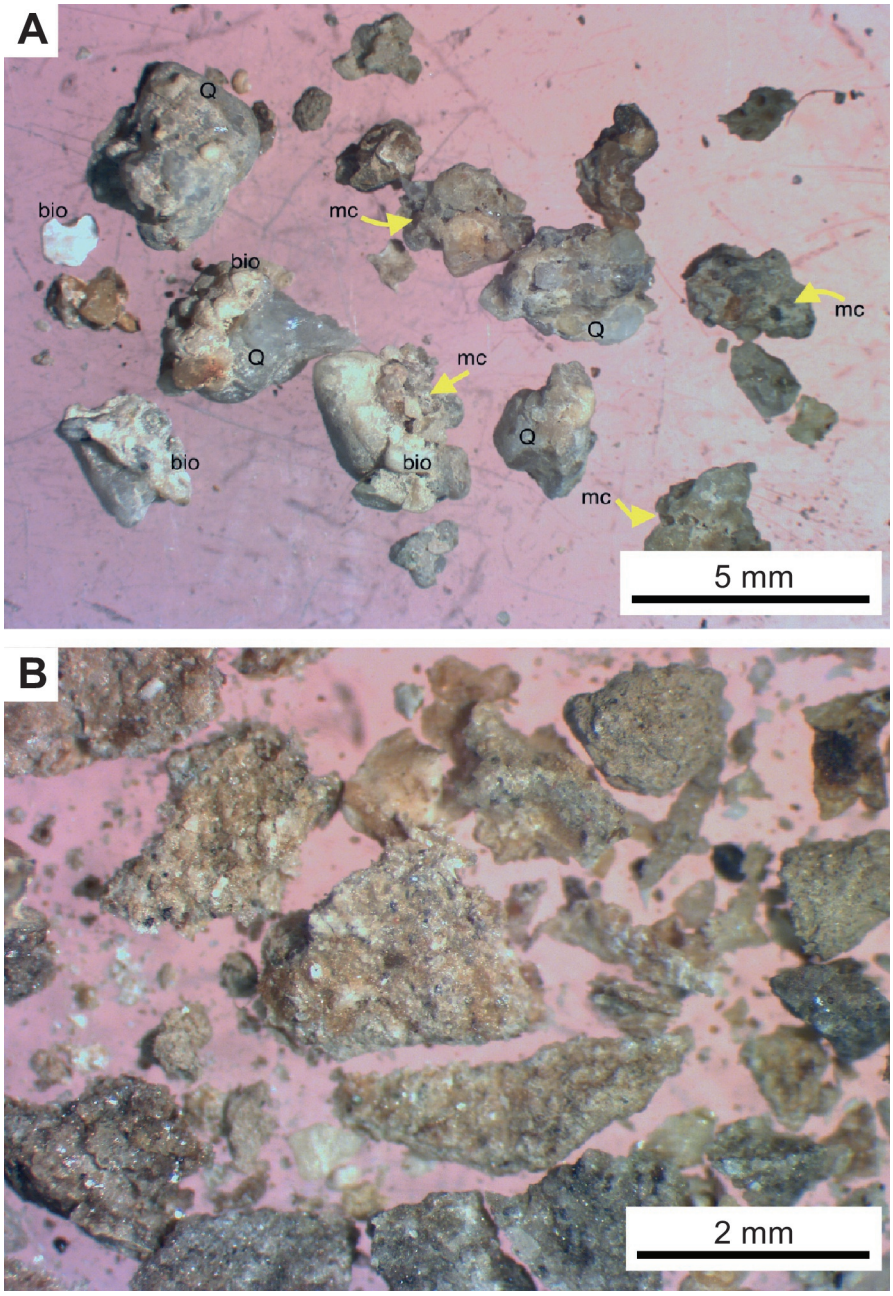

sed_13061_fig. 2.eps

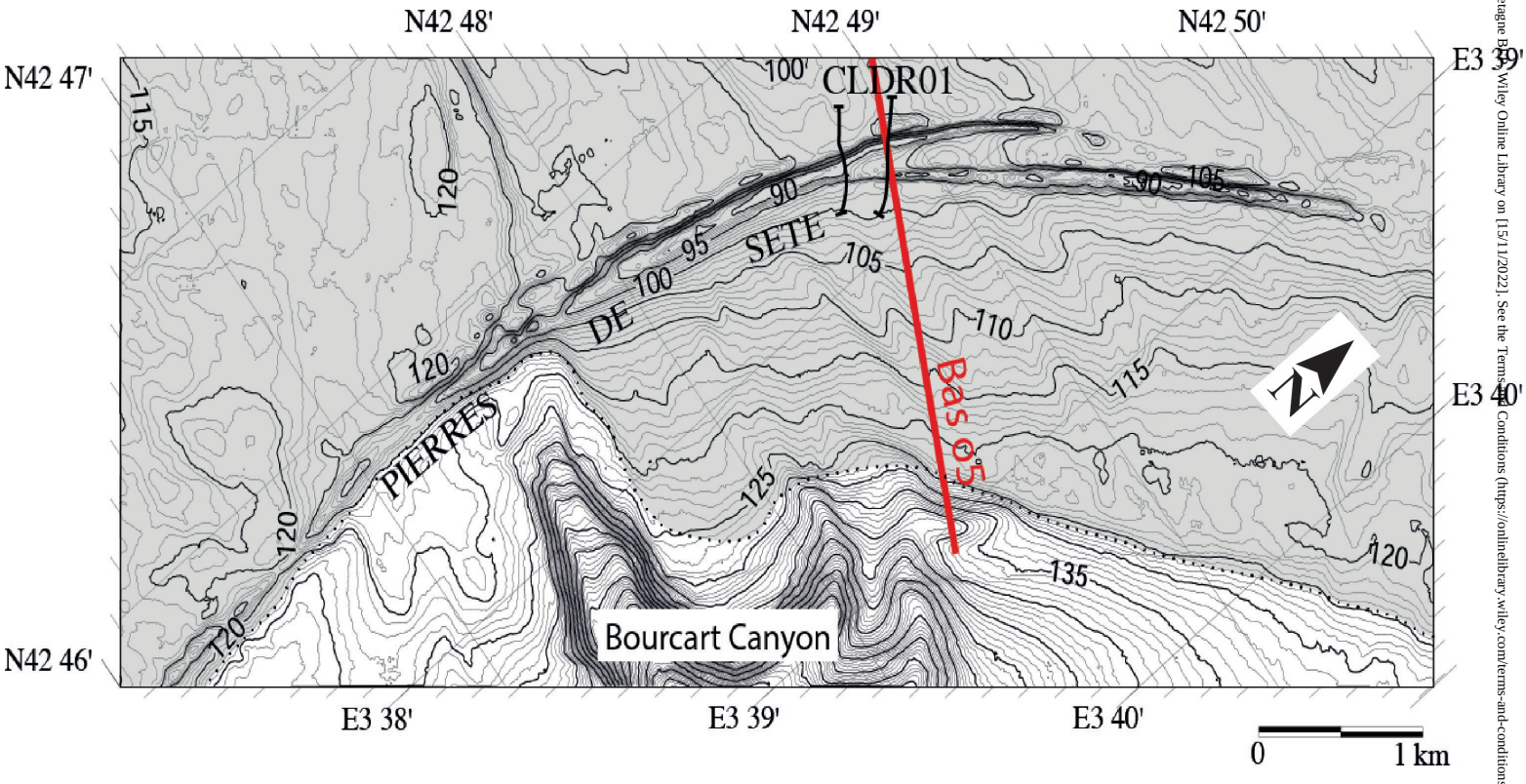

sed_13061_fig. 3.eps

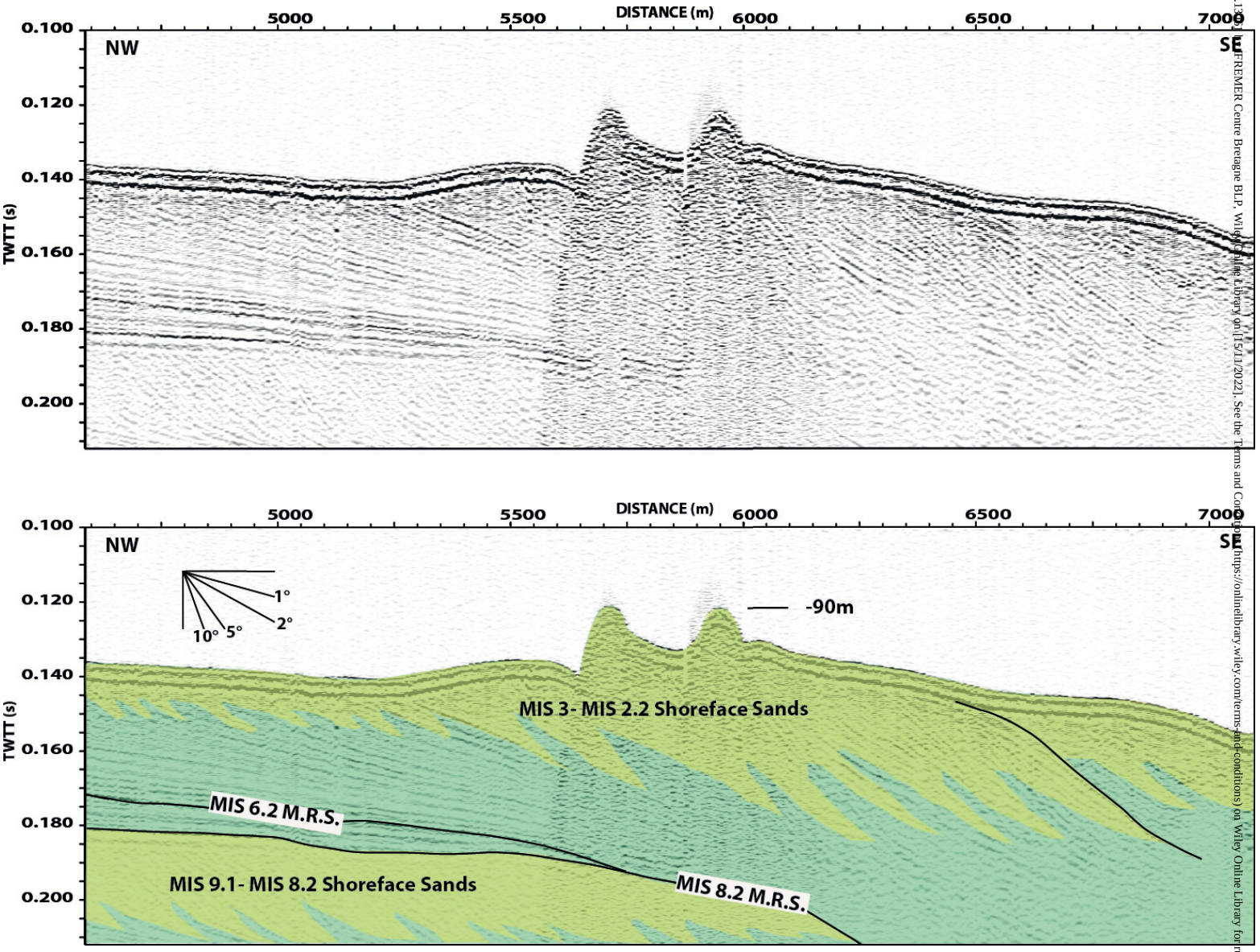

sed_13061_fig. 4.eps

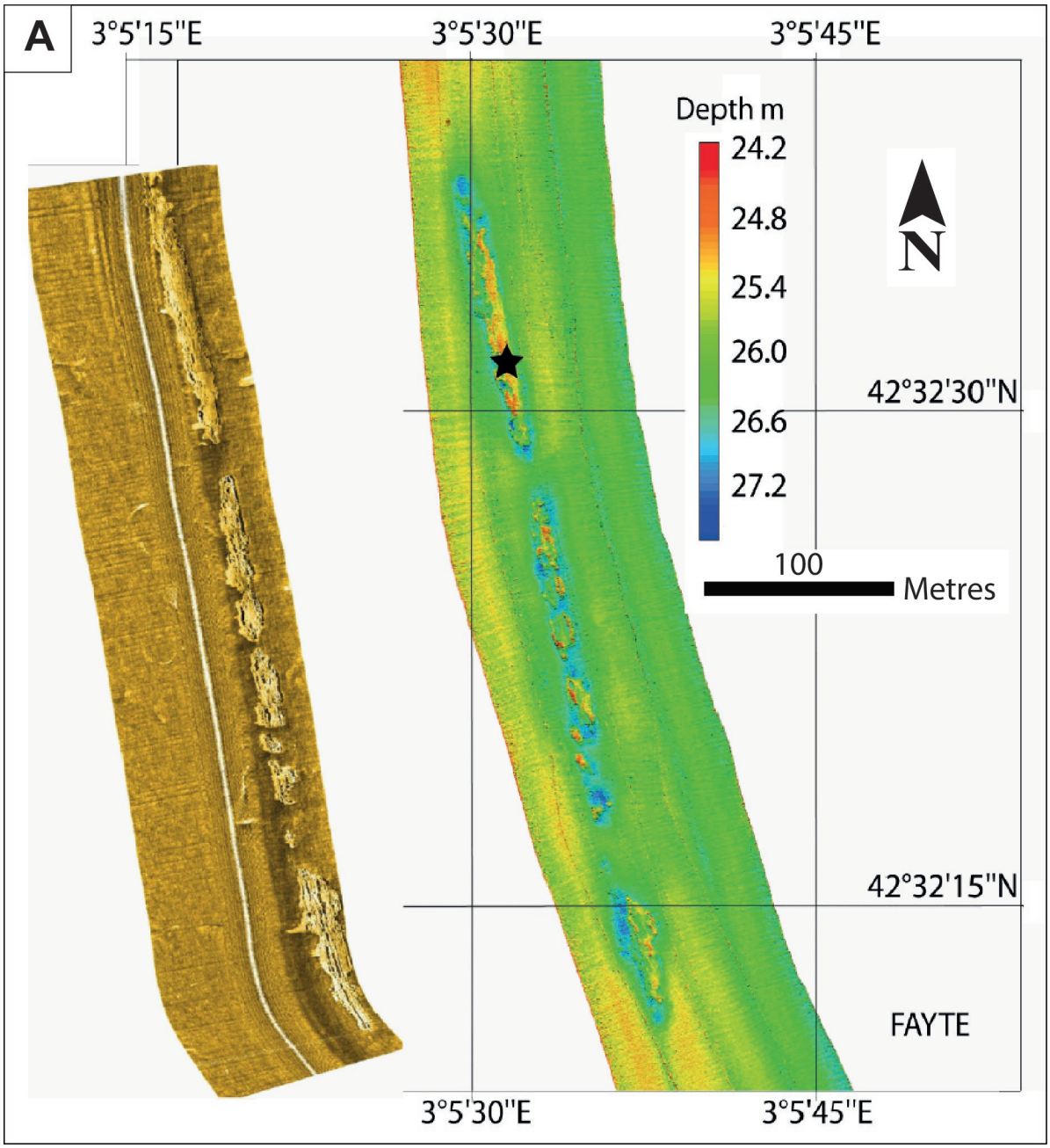

sed_13061_fig. 5a.eps

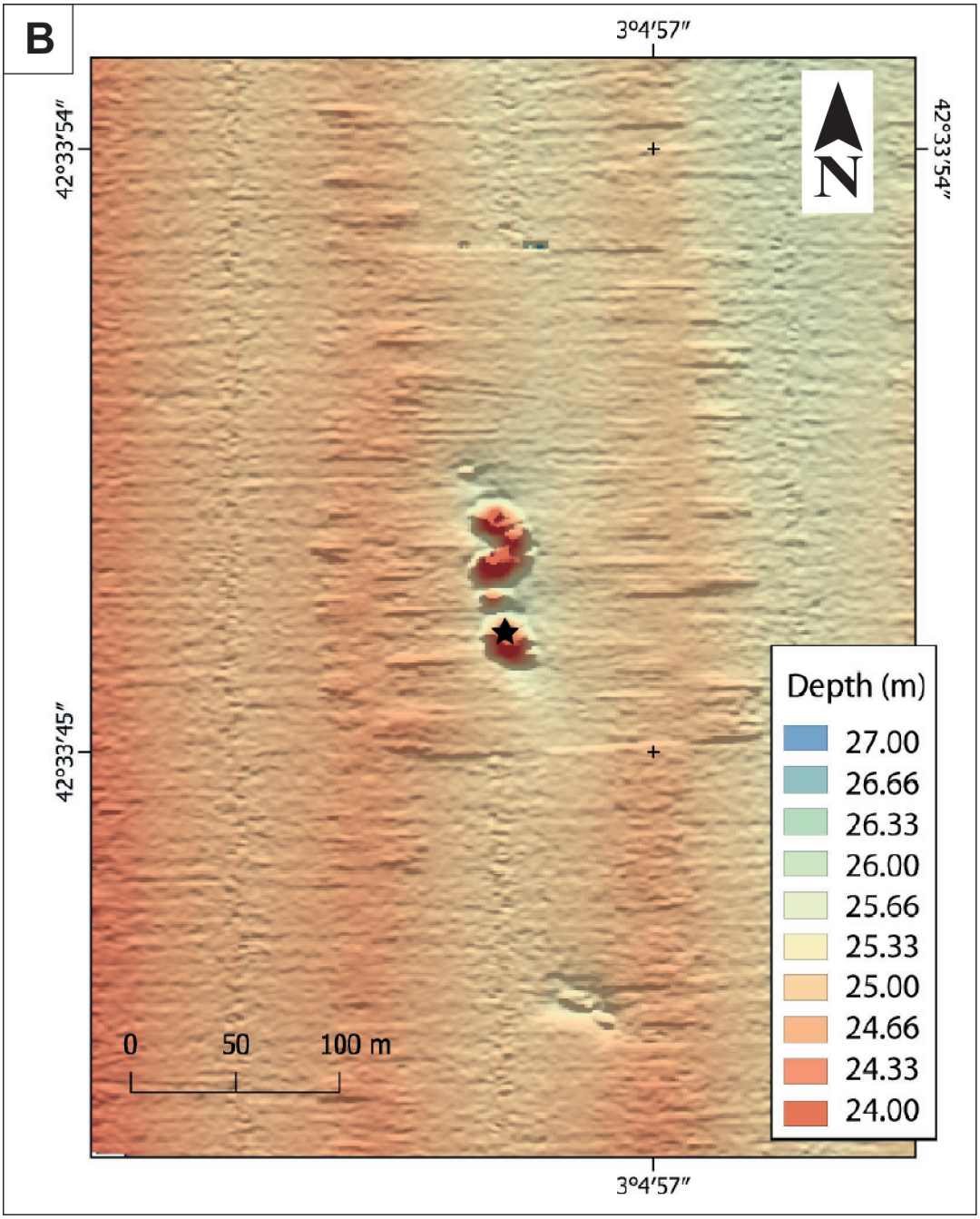

sed_13061_fig. 5b.eps

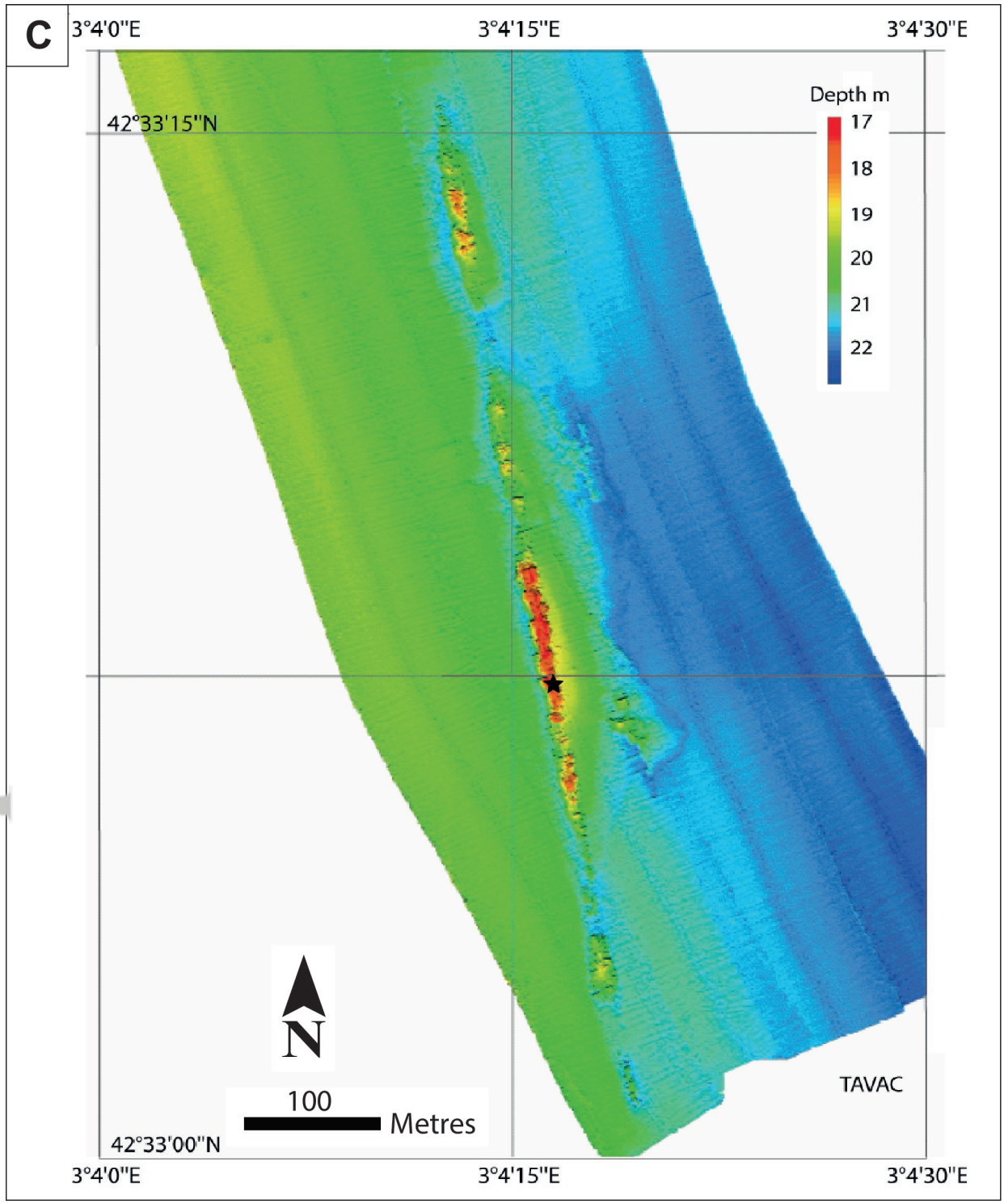

sed_13061_fig. 5c.eps

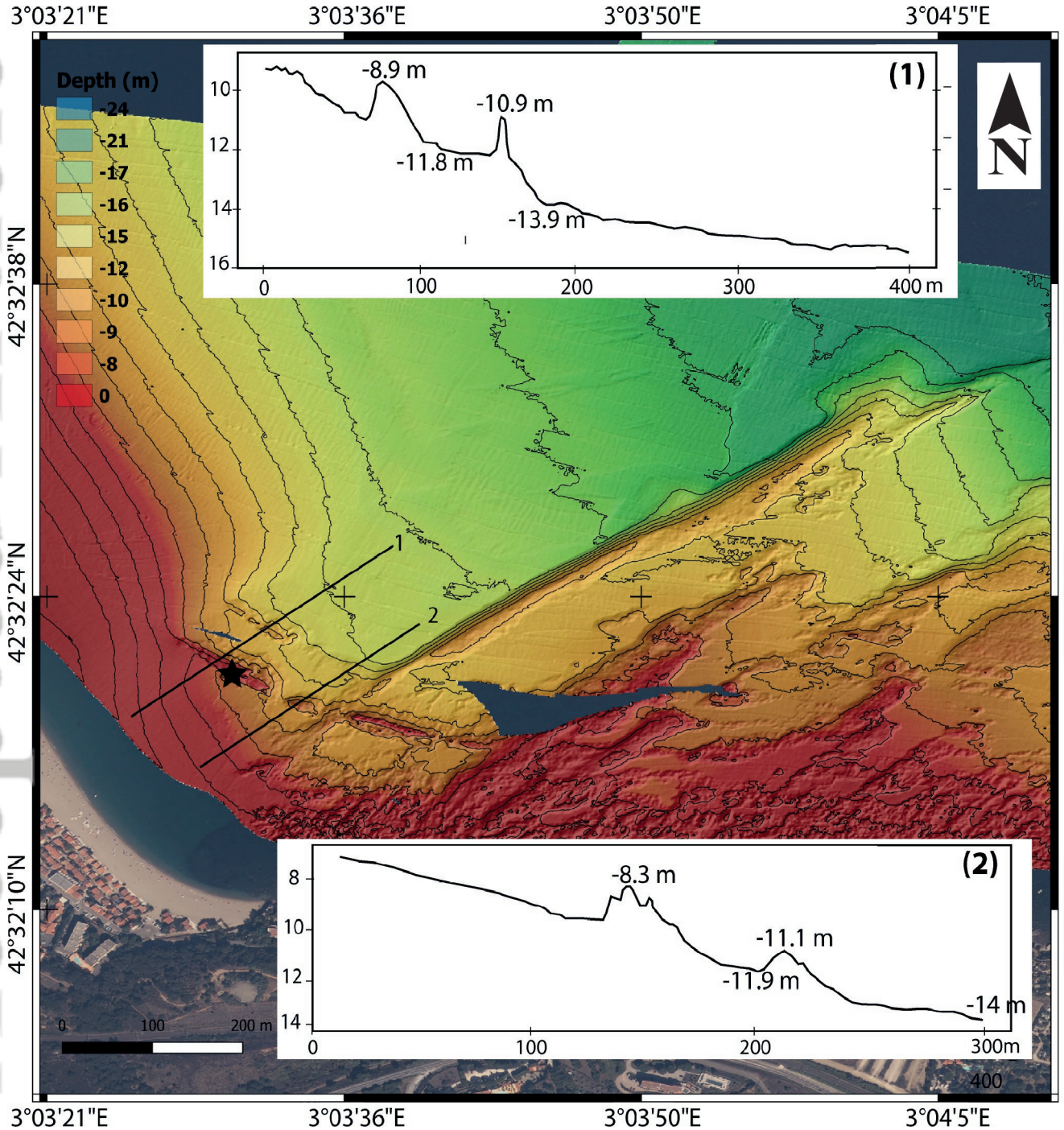

sed_13061_fig. 6.eps

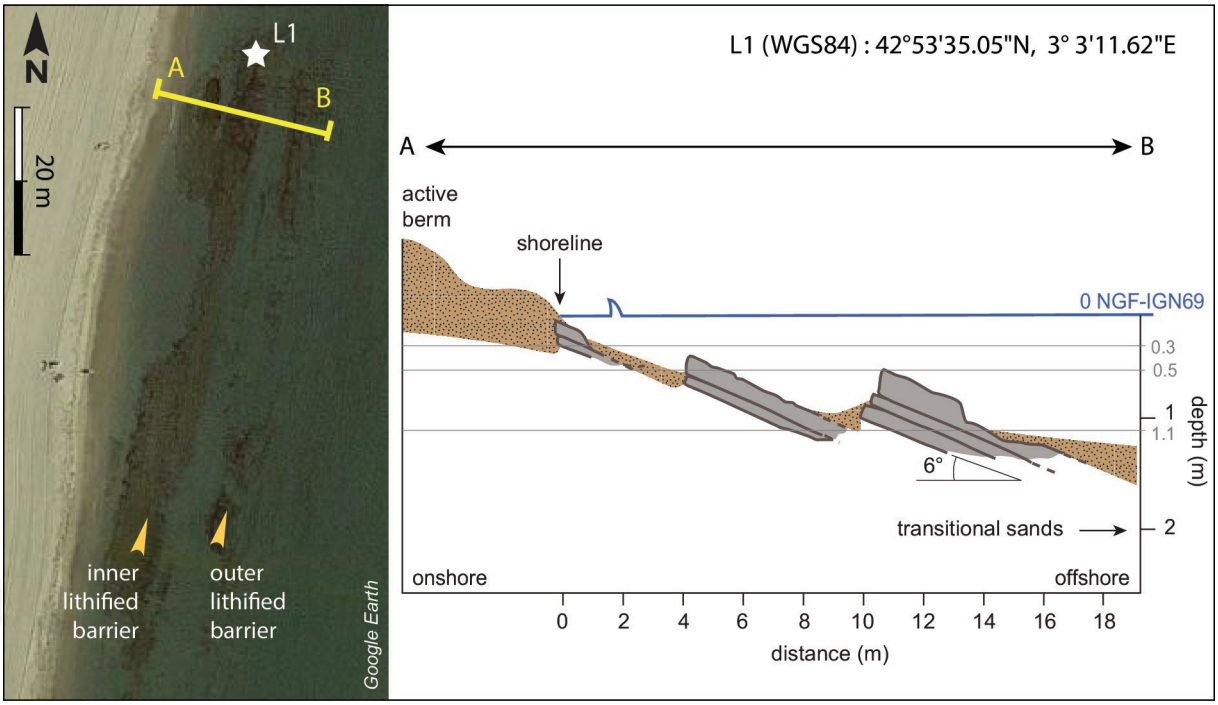

sed_13061_fig. 7.eps

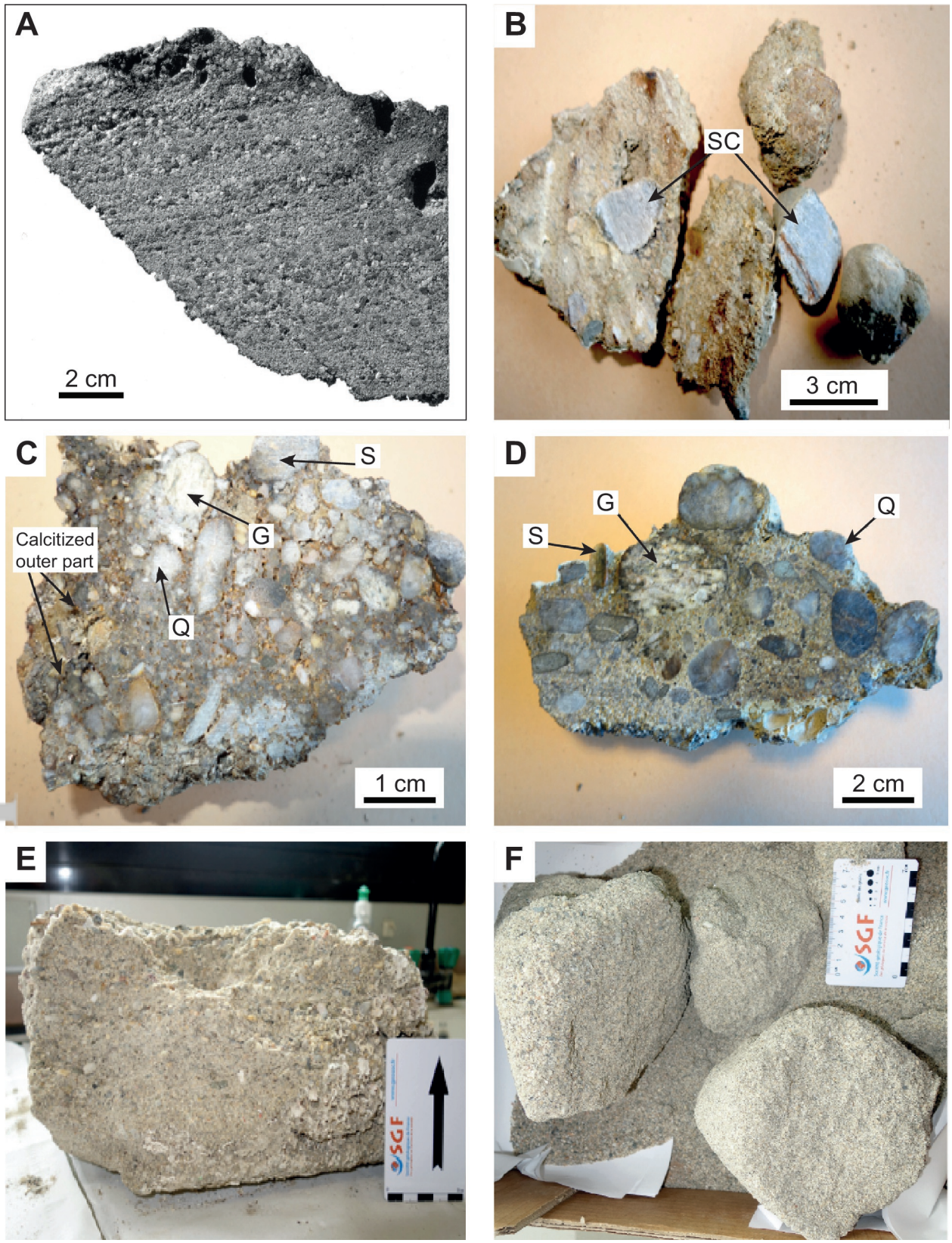

sed_13061_fig. 8.eps

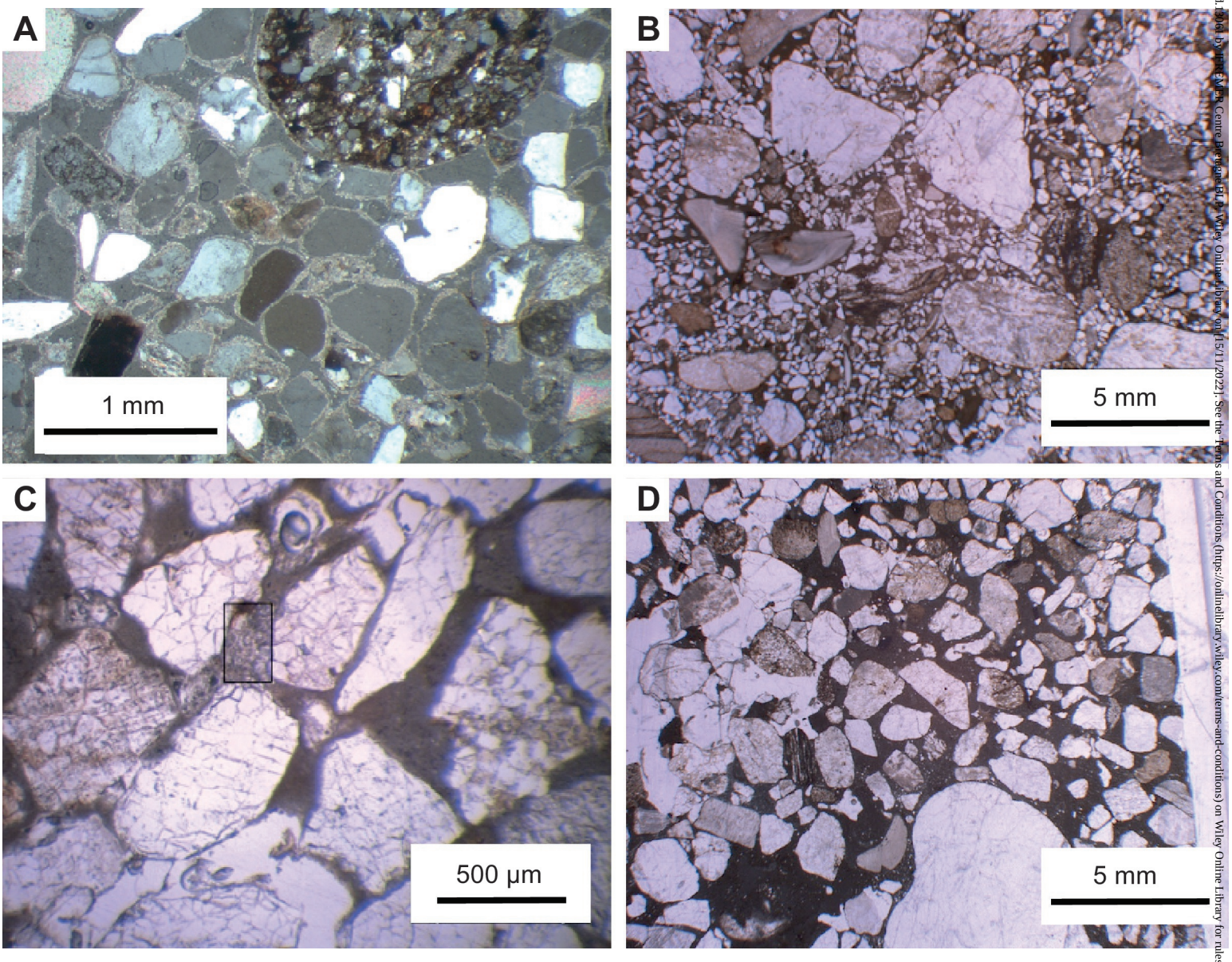

sed_13061_fig. 9.eps

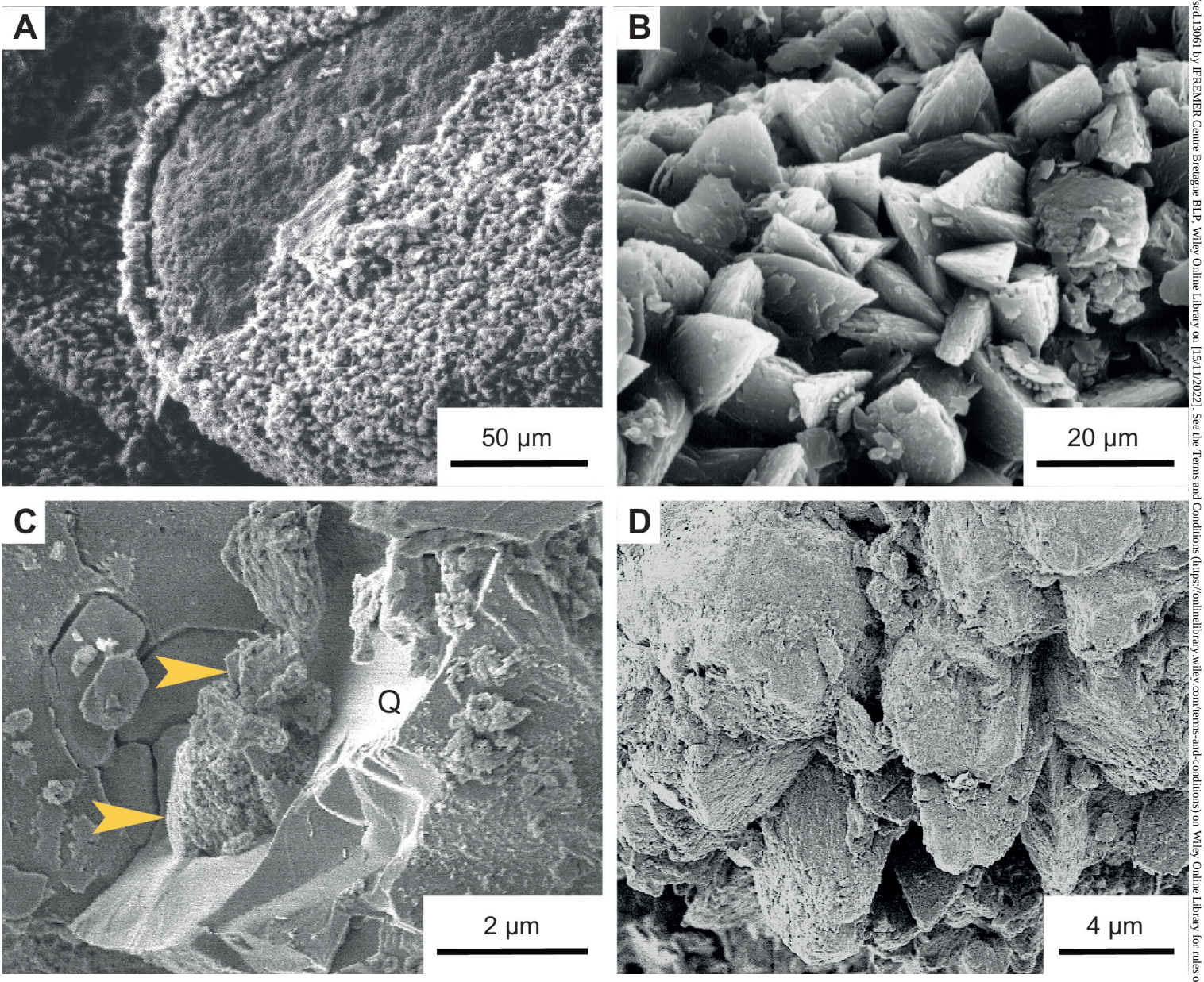

sed_13061_fig. 10.eps

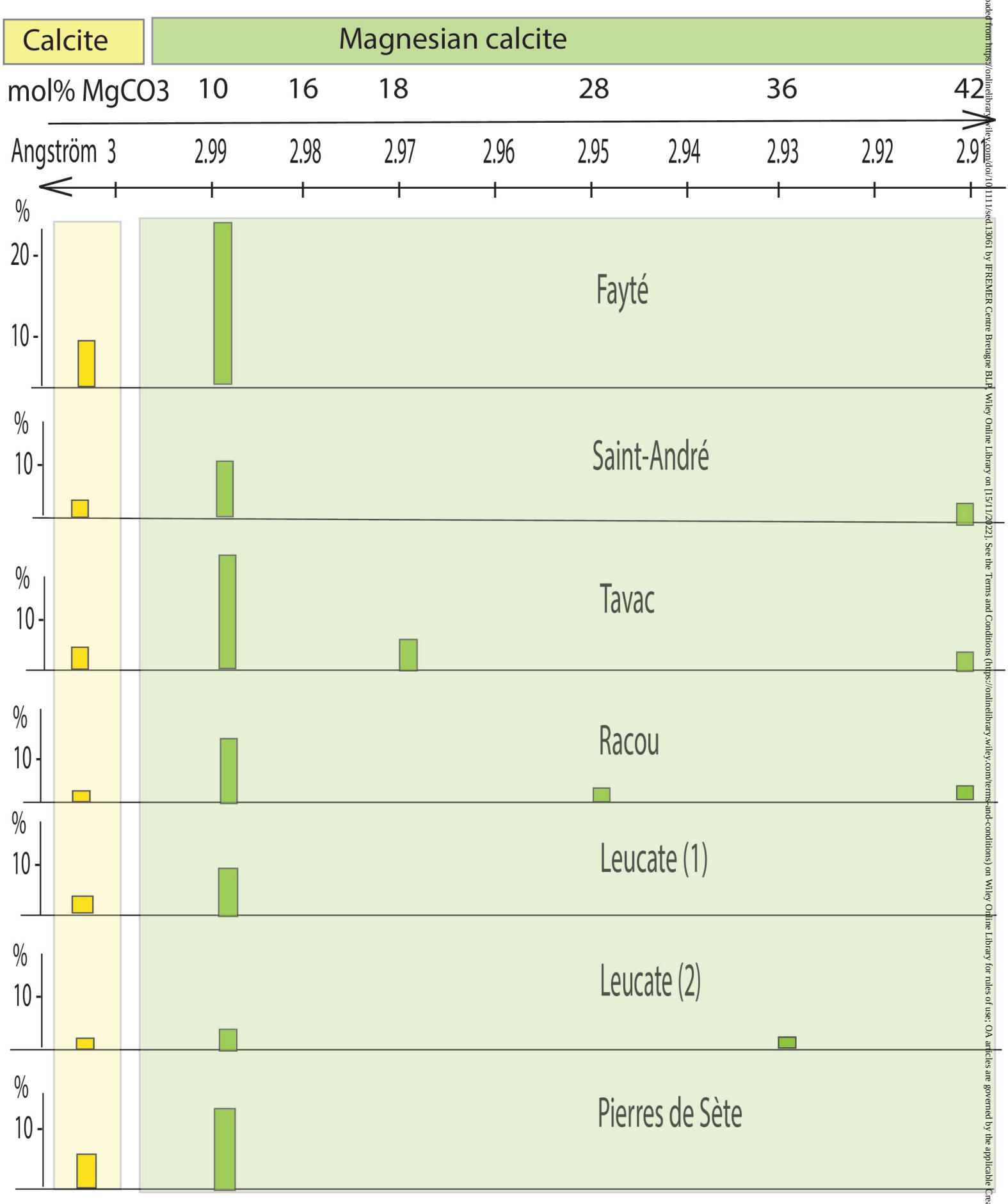

sed_13061_fig. 11.eps

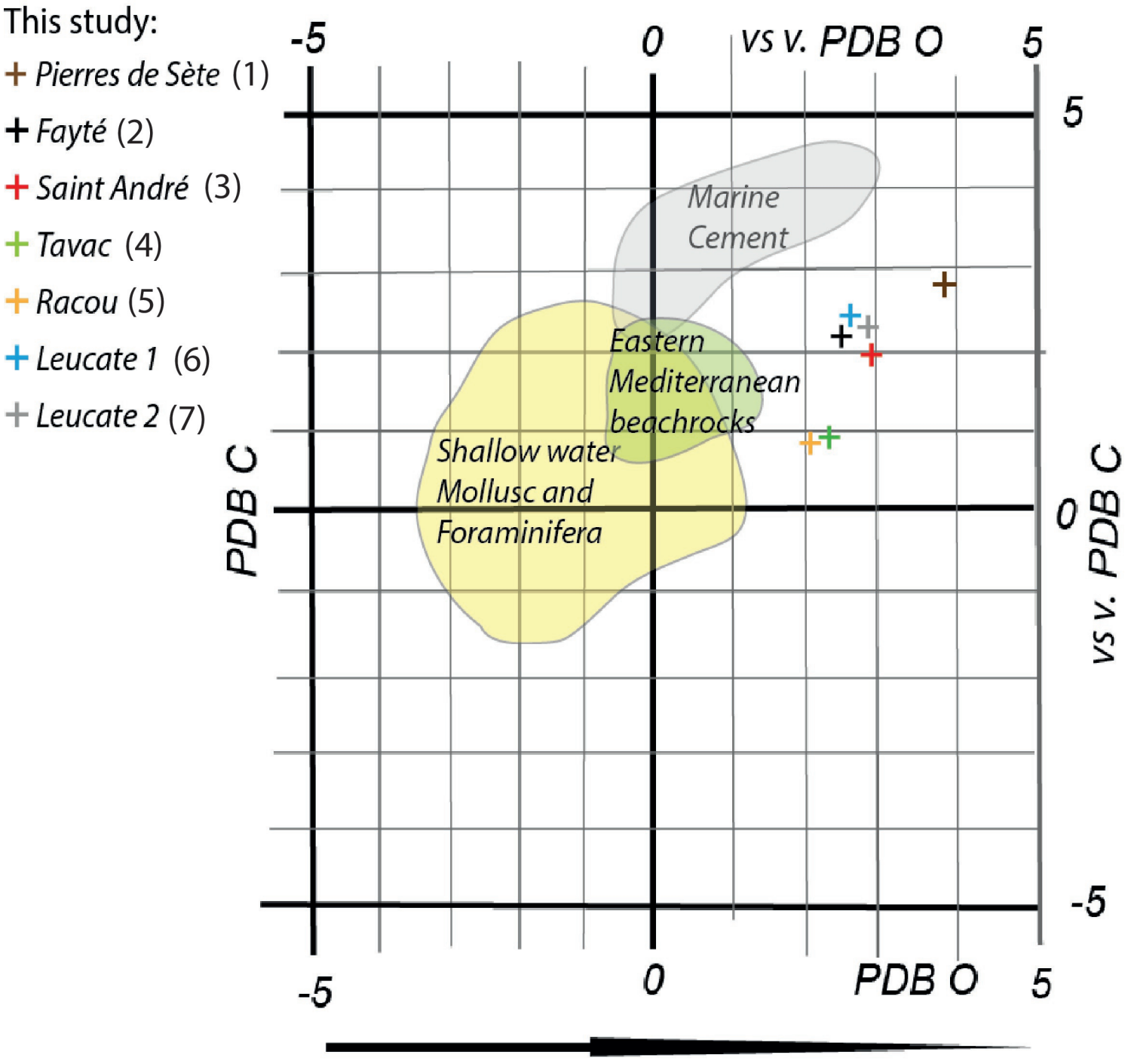

Marine cement field from Andersson and Arthur (1983)
Shallow water Mollusc and Foraminifera field from Tucker and Wright (1990)
Eastern Mediterranean beachrocks field from Holail and Rached (1992)

sed_13061_fig. 12.eps

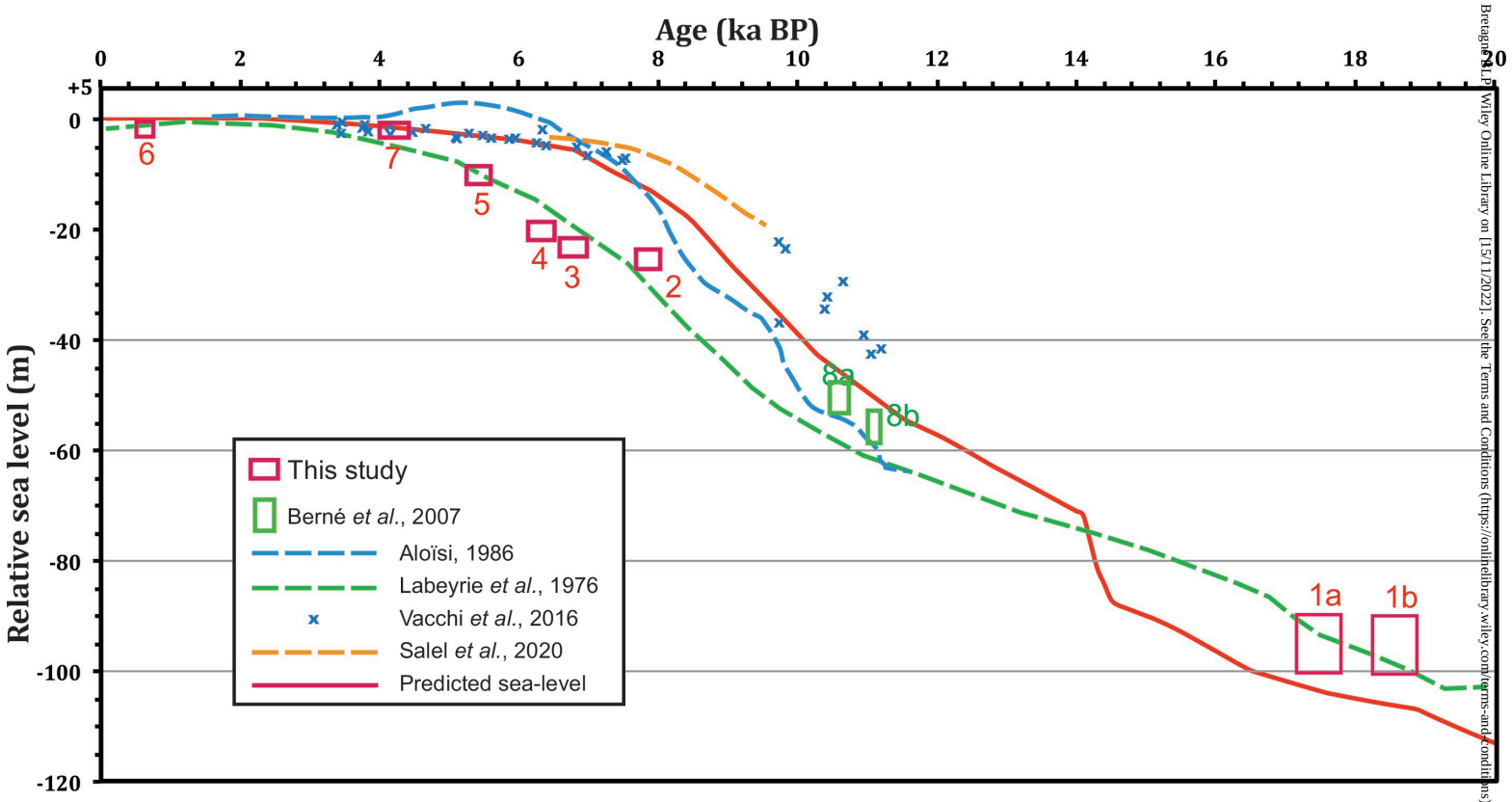

sed_13061_fig. 13.eps